Structural Engineering and Mechanics, *Vol. 64, No. 5 (2017) 621-640*
DOI: https://doi.org/10.12989/sem.2017.64.5.621

Post buckling mechanics and strength of cold-formed steel columns exhibiting Local-Distortional interaction mode failure

Hareesh Muthuraj[1a], S.K. Sekar[*1], Mahen Mahendran[2b] and O.P. Deepak[1]

[1]*School of Civil and Chemical Engineering, VIT University, Vellore, TamilNadu-632014, India*
[2]*School of Civil and Built Environment, QUT, Brisbane, Australia*

(Received July 10, 2017, Revised September 13, 2017, Accepted October 3, 2017)

Abstract. This paper reports the numerical investigation conducted to study the influence of Local-Distortional (L-D) interaction mode buckling on post buckling strength erosion in fixed ended lipped channel cold formed steel columns. This investigation comprises of 81 column sections with various geometries and yield stresses that are carefully chosen to cover wide range of strength related parametric ratios like (i) distortional to local critical buckling stress ratio ($0.91 \leq F_{CRD}/F_{CRL} \leq 4.05$) (ii) non dimensional local slenderness ratio ($0.88 \leq \lambda_L \leq 3.54$) (iii) non-dimensional distortional slenderness ratio ($0.68 \leq \lambda_D \leq 3.23$) and (iv) yield to non-critical buckling stress ratio (0.45 to 10.4). The numerical investigation is carried out by conducting linear and non-linear shell finite element analysis (SFEA) using ABAQUS software. The non-linear SFEA includes both geometry and material non-linearity. The numerical results obtained are deeply analysed to understand the post buckling mechanics, failure modes and ultimate strength that are influenced by L-D interaction with respect to strength related parametric ratios. The ultimate strength data obtained from numerical analysis are compared with (i) the experimental tests data concerning L-D interaction mode buckling reported by other researchers (ii) column strength predicted by Direct Strength Method (DSM) column strength curves for local and distortional buckling specified in AISI S-100 (iii) strength predicted by available DSM based approaches that includes L-D interaction mode failure. The role of flange width to web depth ratio on post buckling strength erosion is reported. Then the paper concludes with merits and limitations of codified DSM and available DSM based approaches on accurate failure strength prediction.

Keywords: lipped channel columns; Local-Distortional interaction; secondary bifurcation; cold formed steel; Direct Strength Method (DSM); numerical simulation; Finite Element Analysis (FEA); Generalized Beam Theory (GBT)

1. Introduction

The cold formed steel (CFS) sections can effectively replace the conventional hot rolled steel sections in light weight steel constructions (Kwon *et al*. 2009). The mostly used CFS sections are of open cross section, fabricated from thin steel sheet with multiple folds and so have slender individual plate elements (i.e., high width to thickness ratio) that constitute the cross section. The high slenderness of individual plate elements make CFS section susceptible to pre-mature (elastic) in-plane deformations (stability issues) namely Local (*L*) and Distortional (*D*) buckling (Dinis *et al*. 2014) under compressive stresses. The behaviour and ultimate strength of CFS sections are governed by pre-mature *L* and *D* buckling, CFS sections generally possess considerable strength reserve post to *L* and *D* buckling called as post buckling strength. The current codified DSM has been proved to provide safe and accurate strength prediction and can be safely employed for the design of CFS columns and beams that fail under *L* or *D* buckling (Dinis *et al*. 2014). However, recent researches have shown that the many of the commonly used open cross section CFS columns exhibit combined L-D buckling mode failure and more importantly with substantial reduction in post buckling strength.

This interaction between *L* and *D* buckling is more promising to occur for those sections with very close *L* and *D* critical buckling stresses, known as true interaction. For sections with considerable difference between *L* and *D* critical stresses, the occurrence of L-D interaction mode buckling depends on the post buckling strength reserve available for the section to reach non-critical buckling stress and the initial geometrical imperfection of the section, known as secondary bifurcation L-D interaction. The post buckling strength erosion stemming from L-D interaction mode buckling is not been addressed by DSM in any of the design specifications of CFS members and thus current DSM provision leads to unsafe strength prediction. In view of this, a quantum of research work devoted to L-D interaction in CFS columns was carried out by researchers around the world to understand its influence on the post buckling behaviour and ultimate strength erosion.

Kwon and Hancock (1992) reported the experimental tests conducted on plain lipped channel and web stiffened lipped channel section columns. Their findings are high strength CFS columns possess significant post buckling strength in the distortional mode and L-D true interaction

∗Corresponding author, Senior Professor
E-mail: sksekar@vit.ac.in
[a]PhD Candidate
[b]Professor

Copyright © 2017 Techno-Press, Ltd.

ISSN: 1225-4568 (Print), 1598-6217 (Online)

mode buckling. Young and Yan (2002) provided experimental evidences for occurrence for combined L-D buckling, combined Local-Distortional-Flexural (L-D-F) buckling & combined Local-Flexural-Torsional (L-FT) buckling in lipped channel columns. Schafer (2002) presented the closed-form prediction of accurate critical buckling stress in L mode & D mode considering the elastic and geometric stiffness of web-flange junction and suggested several design methods for columns prone to fail by various interaction mode buckling. Kwon, Kim and Hancock (2009) based on their experimental investigations on lipped channel and web, flange stiffened lipped channel columns proposed a modified strength equation for columns made of medium strength steel that fails under L-D interaction mode buckling phenomenon. Silvestre, Camotim and Dinis (2009) conducted numerical investigations on lipped channel columns with and simply supported boundary conditions. The authors concluded that the influence of L-D interaction on (i) ultimate strength erosion is minimal and DSM nominal distortional strength curve accurately predicts the ultimate strength for fixed-fixed columns with low to moderate distortional slenderness ratio (λ_D) (ii) ultimate strength erosion is significant and DSM based nominal Local-Distortional strength curve (NLD) approach provides reasonably accurate ultimate strengths for fixed ended columns with moderate to high λ_D (iii) ultimate strength erosion is significant and NLD approach predicts accurately the ultimate strength for all simply supported columns.

Silvestre, Camotim and Dinis (2012) presented the numerical investigation conducted on 276 lipped channel columns and proposed a DSM based modified NDL approach (P^*_{NDL}) for the accurate prediction of ultimate strengths. Young, Silvestre and Camotim (2013) conducted experimental tests on lipped channel columns with critical distortional buckling stress (F_{CRD}) greater than critical local buckling stress (F_{CRL}). The authors reported that DSM based NLD approach predicts the ultimate strength of the column accurately. Dinis, Young and Camotim (2014) reported the experimental and numerical investigations on CFS rack sections and concluded that NLD approach predicts the ultimate strengths accurately. He *et al*. (2014) provided the experimental evidence for occurrence of L-D interaction for web stiffened lipped channel columns having critical stress ratio $0.71 \leq F_{CRD}/F_{CRL} \leq 2.06$ and adequately high yield stress (F_Y). They concluded that the influence of L-D interaction on ultimate strength erosion is significant and both NLD and NDL approach satisfactorily predicts the ultimate strength. Martins *et al*. (2015) conducted numerical investigations on lipped channel and web stiffened lipped channel columns undergoing true and secondary bifurcation kinds of L-D interaction buckling. The authors concluded that the influence of secondary local bifurcation L-D interaction on ultimate strength erosion is insignificant and DSM nominal distortional buckling strength curve provides accurate estimate, whereas, for true and secondary distortional bifurcation L-D interaction NDL approach provides accurate results for both plain lipped and web stiffened lipped channel sections. Martins *et al*. (2015) studied the suitability of DSM based NDL and Modified NDL (MNDL) approaches in predicting the accurate ultimate strength of columns affected by L-D interaction mode buckling by conducting numerical investigations on lipped channel, hat, Zed and rack section columns. They reported both NDL and MNDL predicted safe and accurate ultimate strengths. Martins, Dinis and Camotim (2016) presented the numerical investigations of web stiffened lipped channel sections where the strength erosion stemming from flange triggered local-distortional interaction buckling is studied. The authors concluded that NDL approach provides safe and accurate estimates of strength and MNDL cannot predict accurate estimates.

This paper presents the numerical investigation and DSM based design of fixed ended lipped channel section columns that fail after L-D interaction buckling. The literature study presented above clearly shows the importance of the need for more reliable DSM based design equation to cater the influence of L-D interaction on ultimate strength erosion of CFS columns. A decent amount of research concerning L-D interaction is carried out more in the form of numerical investigation and from available results it can be noted that the DSM based NLD and NDL approaches can able to satisfactorily capture the strength erosion due to L-D interaction effect. The both NLD and NDL approach of design was firstly suggested by Schafer (2002), amongst them NLD is first adopted by Yang and Hancock (2004) in their work and later based on their experimental test results, they modified the NLD equation to account for the higher strength degradation due to L-D interaction observed particularly for columns made from medium strength steel. However, the experimental tests conducted by the Hancock *et al.* are only on limited columns and hence further verification on accuracy of proposed equation is required to be carried out for large numbers of column to cover wide range of parameters on which L-D interaction may strongly rely.

The NDL design approach is intensively verified by Camotim *et al.* (2009, 2012, 2014, 2015, 2016) against their numerical investigation conducted on large numbers of plain lipped channel, web or flange stiffened lipped channel, hat, rack and Zed section columns failing after true and secondary bifurcation kinds L-D interaction phenomena. They identified the NDL approach suggested by Schafer provides over conservative strength prediction for stocky columns (λ_D<1.5) and conservative results for most of the slender columns ($\lambda_D \geq 1.5$) and hence proposed a modified NDL equation for more accurate prediction of ultimate strength. However, these findings are reported based on non-linear post buckling finite element analysis conducted by considering only pure distortional mode (identified to be detrimental in few sections) as initial geometric imperfection with small imperfection magnitude of 0.1 times of thickness (0.1T) of section. This has to be revisited because to obtain exact simulation of failure modes and ultimate loads using finite element analysis (FEA) as that of experimental tests conducted, Dinis *et al.* (2014), He *et al.* (2014), Kumar *et al.* (2014), Anbarasu (2016) have adopted much higher imperfection magnitude on comparison to 0.1T.

In view to provide additional contribution to the current

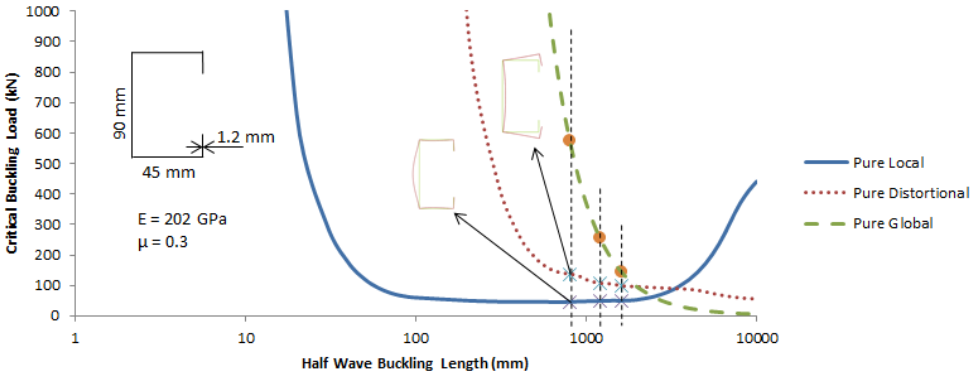

Fig. 1 Column critical buckling curves obtained from GBTUL

research findings, this paper is aimed at to explore the key parameters (related to strength and cross section dimension) that governs the degree of influence the L-D interaction have on post buckling strength degradation. A total of 81 lipped channel sections covering wide range of strength related parametric ratios like (i) distortional to local critical buckling stress ratio ($0.91 \leq F_{CRD}/F_{CRL} \leq 4.05$) (ii) non-dimensional local slenderness ratio ($0.88 \leq \lambda_L \leq 3.54$) (iii) non-dimensional distortional slenderness ratio ($0.68 \leq \lambda_D \leq 3.23$) and (iv) yield to non-critical buckling stress ratio (0.45 to 10.4) are presented in this study. The methodology adopted for this study are (i) identification of column geometries corresponding to wide range of parametric ratios by conducting linear buckling analysis using open source GBTUL program developed at University of Lisbon, (ii) linear buckling analysis for identified column sections using ABAQUS (FEA package), this is performed to obtain different eigenmodes that can be conveniently incorporated as initial geometrical imperfection for post buckling analysis, (iii) non-linear buckling analysis (with material and geometrical non-linearity's) in ABAQUS to understand the post buckling mechanics and to obtain the failure load data, (iv) comparison of ultimate strength data obtained through FEA with nominal strength predicted from current DSM (L & D buckling) and with strength predicted from other DSM based NLD, NDL & MNDL approaches reported in the literatures.

2. Column geometry identification

The identification of different column geometries for fixed ended condition is achieved by conducting large numbers of iterative buckling analysis in an open source GBTUL program. The GBTUL program performs buckling analysis for thin walled sections based on Generalized Beam Theory (GBT) developed by Bebiano *et al.* (2008). One of the greatest advantages of using GBTUL is that critical buckling loads for pure *L*, *D* and *G* modes can be obtained directly by defining the deformation modes of interest and boundary conditions. However, the difficult task is to ensure the occurrence of L-D interaction for the chosen section. Atleast, it is possible to a certain extent to know the possibilities for L-D true interaction to occur for a section from the critical buckling curves of pure *L* and *D* modes. Fig. 1 shows the plot for critical buckling load *Vs* column length/half wave buckling length for a section mentioned within. For instance, from Fig. 1 it can be noted that at 3500 mm length where both pure *L* and *D* modes critical stresses meet, the column can be expected to incur L-D true interaction at this particular length (note that critical buckling load for pure global mode is very less compared to that of pure L & D mode at this length, so the column is to obviously fail by global buckling). But for L-D secondary bifurcation interaction, there are no specific ways to visualize the possibilities for occurrence of this interaction. Hence in this work, length of a section is first chosen arbitrarily where the critical loads for pure *L* and *D* mode are distinct and well below the pure *G* mode Then linear buckling analysis and non- linear post buckling analysis is carried out in FEA to ensure the occurrence of either L-D true or secondary bifurcation kinds of interaction. Recently, Martins *et al.* (2015) employed non-linear GBT formulations to simulate the load-deflection equilibrium path post to elastic buckling for various combinations of deformation modes to identify the possibility of L-D interactions. In this paper, only the column geometry that fails after L-D interaction are been reported. The details of the section geometry, critical buckling stresses and stress ratios are presented in the Table 1.

3. Finite element modelling

The identified lipped channel column sections are modelled as 4 node shell elements (S4R5) with reduced integration rule and 5 degrees of freedom per node available in ABAQUS. Finite element mesh of length to width ratio 1 is adopted based on the convergence study. The ends of the column are connected to solid plates using tie constraint between the inner face of the plate and shell edges of the section. The solid plate is modelled using deformable solid element C3D8R with reference to He *et al.* (2014). The solid plates are assigned with fixed boundary conditions (i.e., null displacements and rotations along *X*, *Y* & *Z* coordinates) on two sides of each plate (XZ & YZ planes). The longitudinal displacement alone is set unrestrained for the top plate. The compressive load is applied as static pressure through the top plate with an initial magnitude of 1

Table 1 Specimen Id, cross sectional dimensions, thickness & length (in mm), area (mm^2), critical buckling stresses (in MPa) & critical stress ratios

Specimen	B_w	B_f	B_s	T	L	Area	F_{CRL}	F_{CRD}	F_{CRE}	F_{CRD}/F_{CRL}	F_{CRE}/F_{CRD}
LS-1-800					800		127.6	175.9	1431.3	1.38	8.14
LS-1-1200	65	86	10	1.0	1200	257	134.4	143.5	637.7	1.07	4.44
LS-1-1600					1600		138.3	127.9	359.9	0.92	2.81
LS-2-800					800		161.5	213.3	1506.0	1.32	7.06
LS-2-1200	70	70	10	1.0	1200	230	169.7	168.5	671.4	0.99	3.99
LS-2-1600					1600		171.5	156.1	379.3	0.91	2.43
LS-3-800					800		126.9	215.2	2914.6	1.70	13.54
LS-3-1200	105	70	10	1.0	1200	318	133.3	170.3	1298.1	1.28	7.62
LS-3-1600					1600		138.4	158.2	732.5	1.14	4.63
LS-4-800					800		183.7	547.4	2280.4	2.98	4.17
LS-4-1200	90	45	15	1.2	1200	252	195.7	426.6	1018.7	2.18	2.39
LS-4-1600					1600		198.3	394.1	577.2	1.99	1.46
LS-5-800					800		44.6	87.9	4986.7	1.97	56.72
LS-5-1200	135	130	10	1.0	1200	415	44.0	58.7	2216.5	1.34	37.73
LS-5-1600					1600		45.1	52.9	1247.2	1.17	23.59
LS-6-800					800		280.0	370.2	1141.3	1.32	3.08
LS-6-1200	60	45	10	1.0	1200	170	287.4	321.5	511.7	1.12	1.59
LS-6-1600					1600		324.8	303.5	291.3	0.93	0.96
LS-7-800					800		90.0	364.2	3506.9	4.05	9.63
LS-7-1200	130	50	15	1.2	1200	312	91.7	294.7	1561.7	3.21	5.30
LS-7-1600					1600		95.9	271.0	881.5	2.83	3.25
LS-8-800					800		123.6	460.9	2756.7	3.73	5.98
LS-8-1200	110	44	15	1.2	1200	273.6	130.9	362.1	1229.9	2.77	3.40
LS-8-1600					1600		136.3	335.4	695.8	2.46	2.07
LS-9-800					800		92.3	314.2	4201.1	3.40	13.37
LS-9-1200	125	75	15	1.2	1200	366	93.7	250.4	1868.8	2.67	7.46
LS-9-1600					1600		97.8	203.6	1052.9	2.08	5.17

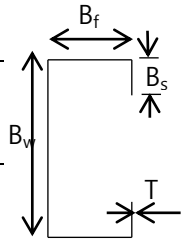

Table 2 Validation of present FEA model against the FEA model from Silvestre *et al*. (2012)

ST-3 Section						Silvestre *et al.* (2012)			Present FEA model			Comparison		
B_w	B_f	B_s	T	L	Yield Stress	F_{CRL}	F_{CRD}	F_U	F_{CRL}	F_{CRD}	F_U	Col 7/	Col 8/	Col
1	2	3	4	5	(F_Y) 6	7	8	9	10	11	12	10	11	9/12
100	100	22	2	1600	250	319	338	235	326.6	340.7	226.9	0.97	0.99	1.03

N/mm^2. The material is defined as isotropic and homogeneous with elastic modulus value of 202 GPa and Poisson's ratio 0.3 for linear buckling analysis and that for non-linear post buckling analysis, ideal elastic-plastic behaviour is modelled in addition. To assess the accuracy of adopted finite element modelling method in this study, linear buckling and non-linear post buckling analysis are carried out for a section (ST-3) reported by Silvestre *et al.* (2012) and the comparison of results are shown in Table 2. The comparison shows the present model can closely simulate the critical buckling stresses, failure load and failure mode reported by Silvestre *et al.* (2012).

3.1 Initial geometrical imperfection

Strength of a cold formed steel member is particularly sensitive to imperfections in the shape of its eigenmodes (Schafer and Pekoz 1998). Number of methods to include geometrical imperfections in the post buckling analysis are suggested by researchers like Schafer and Pekoz (1998), Dinis *et al.* (2007), Schafer *et al.* (2010), Zeinoddini and Schafer (2012), Sadovsky *et al.* (2012). Though, there are many methods available to define the geometrical imperfections in FEA to trigger the instabilities in the post buckling analysis, the eigenmode based imperfection is convenient one. In this work, twenty different buckling modes (mostly first twenty eigenmodes without linear superposition) obtained from elastic buckling FEA analyses are considered for geometrical imperfection in each of the sections. The buckling modes considered for imperfection includes pure *L*, pure *D* and combined L-D modes with different numbers of *L*, *D* half wave buckling. The magnitude of imperfection is considered as equivalent to plate thickness (1T) as suggested by Schafer and Pekoz (1998). It is important to note that Dinis *et al.* (2014), He *et al.* (2014), Kumar *et al.* (2014), Anbarasu (2016) have used

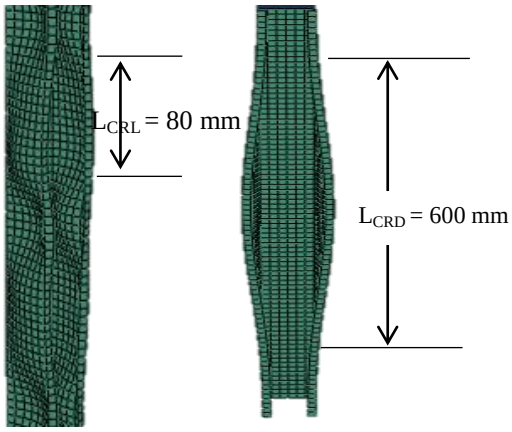

Fig. 2 L_{CRL} & L_{CRD} of section LS-1-800

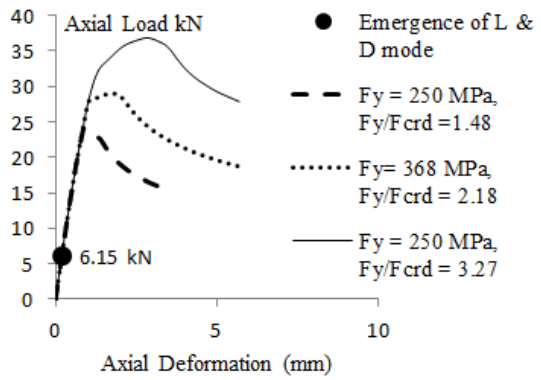

(a) Axial deformation versus axial load

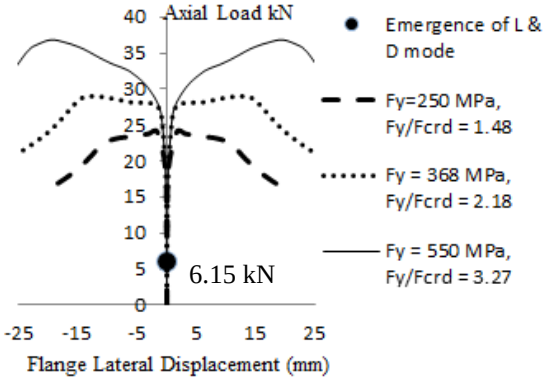

(b) Flange lateral deformation versus axial load

Fig. 3 Load versus deformation plot for section LS-2-1200

the magnitude of imperfection close to 1T to simulate exact experimental test results in FEA.

4. Post buckling mechanics

The post buckling analysis is carried out by defining the non-linear material property as ideal elastic-plastic stress-strain constitutive model. As most of the sections identified in this study have considerable difference between critical *L* and *D* buckling stresses, the yield stress to non-critical stress ratio of the section may play significant role on the post buckling mechanics and failure load. To explore on this, the post buckling analyses are performed for each section with three different yield stresses 250, 368 and 550 MPa. The geometrical non-linearity for the column sections are defined by assigning perturbed mesh based on the eigenmodes obtained from linear buckling analysis. The non-linear post buckling analyses for each section are carried out with twenty different eigenmodes as geometrical imperfection individually, without any linear superposition of different eigenmodes, to identify the most unfavourable mode that leads to least failure load of the columns. The identified most unfavourable imperfection modes for the many of the sections are combined L-D mode (with local buckling in web and flange) rather than pure *D* mode which was considered to be detrimental mode by Silvestre, Camotim and Dinis (2009). The critical half wave buckling lengths for local (L_{CRL}), distortional (L_{CRD}) buckling, length of the column to critical half wave buckling length (L_{CRL} & L_{CRD}) ratio, L_{CRD} to L_{CRL} ratio and most unfavourable imperfection modes with buckling half wave numbers for all the sections are given in Table 3.

The critical half wave buckling lengths L_{CRL} & L_{CRD} are obtained from GBTUL program, L_{CRL} & L_{CRD} denotes the half wave buckling length or indirectly the column length at which, for a section, the critical local and distortional buckling stress is minimal respectively. Fig. 2 shows the lengths of half wave local and distortional buckling for section LS-1-800. All column sections considered in this study have lengths greater than L_{CRD} and so can be categorised as intermediate length columns.

4.1 Buckling behaviour

This Section addresses the post buckling behaviour of columns that are influenced by L-D interaction mode phenomenon. To study the buckling behaviour carefully the column sections are classified into three types based on the type of L-D interaction and yield to non- critical buckling stress ratio. Type 1 sections represent the columns with critical stress ratio in the range of $0.9 \le F_{CRD}/F_{CRL} \le 1.2$, that is sections failing after true L-D interaction. Type 2 sections consists of columns having yield to non- critical buckling stress ratio greater than 1 (F_Y/F_{CRD} or $F_{CRL}>1$) and failing after secondary bifurcation L-D interaction phenomenon. Type-3 sections consists of columns having yield to non-critical buckling stress ratio lesser than 1 (F_Y/F_{CRD} or $F_{CRL}<1$) and failing after secondary bifurcation L-D interaction phenomenon.

4.1.1 Type 1 sections

The sections LS-1-1200, LS-1-1600, LS-2-1200, LS-2-1600, LS-3-1600, LS-5-1600, LS-6-1200 & LS-6-1600 have critical buckling stress ratios between $0.9 \le F_{CRD}/F_{CRL} \le 1.2$. Fig. 3(a) and (b) depicts the load versus deformation equilibrium path for section LS-2-1200 with three different yield stresses. The FEA post buckling analysis for section LS-2-1200 is carried out at minimal fixed load increment rate (0.01) with initial static pressure as 1N/mm^2 to identify the exact loads at emergence of *L* & *D* mode. As the section LS-2-1200 have F_{CR}/F_{CRL} ratio 0.99, the emergence of *L* & *D* mode at same load of 6.15 kN is observed as indicated in Fig. 3. Here, the *L* and *D* buckling are considered as emergent when their deformation magnitude is equivalent

Table 3 Critical half wave local, distortional buckling lengths, critical length ratios and most unfavourable imperfection modes

Section Id	L_{CRL}	L_{CRD}	Length/L_{CRL}	Length/L_{CRD}	L_{CRD}/L_{CRL}	Most unfavourable imperfection modes
LS-1-800			10	1.33		2 HwD + 3 HwL on web + 5 HwL on flange
LS-1-1200	80	600	15	2	7.5	16 HwL on web + 16 HwL on flange
LS-1-1600			20	2.67		4 HwD + 23 HwL on web + 23 HwL on flange
LS-2-800			11.43	1.57		2 HwD + 14 HwL on web + 14 HwL on flange
LS-2-1200	70	510	17.14	2.35	7.29	3 HwD + 18 HwL on web + 18 HwL on flange
LS-2-1600			22.86	3.14		26 HwL on web and flange
LS-3-800			9.09	1.6		1 HwD + 14 HwL on web + 7 HwL on flange
LS-3-1200	88	500	13.64	2.4	5.68	4 HwD + 2 HwL on web
LS-3-1600			18.18	3.2		14 HwL on web + 14 HwL on flange
LS-4-800			11.11	1.6		2 HwD
LS-4-1200	72	500	16.67	2.4	6.94	15 HwL on web + 11 HwL on flange
LS-4-1600			22.22	3.2		21 HwL on web + 11 HwL on flange
LS-5-800			5.93	0.94		1 HwD + 7 HwL on web + 7 HwL on flange
LS-5-1200	135	850	8.89	1.41	6.3	2 HwD + 4 HwL on web + 4 HwL on flange
LS-5-1600			11.85	1.88		14 HwL on web + 14 HwL on flange
LS-6-800			16	2.11		1 HwD + 21 HwL on web + 21 HwL on flange
LS-6-1200	50	380	24	3.16	7.6	4 HwD + 31 HwL on web + 31 HwL on flange
LS-6-1600			32	4.21		4 HwD + 27 HwL on web + 27 HwL flange
LS-7-800			8	1.39		1 HwD + 2 HwL on web
LS-7-1200	100	575	12	2.09	5.75	3 HwD + 2 HwL on web
LS-7-1600			16	2.78		9 HwL on web + 9 HwL on flange
LS-8-800			9.41	1.57		2 HwD + 2 HwL on web
LS-8-1200	85	510	14.12	2.35	6.0	3 HwD + 2 HwL on web
LS-8-1600			18.82	3.14		12 HwL on web + 12 HwL on flange
LS-9-800			8	1.09		1 HwD + 18 HwL on web + 18 HwL on flange
LS-9-1200	100	735	12	1.63	7.35	2 HwD
LS-9-1600			16	2.81		10 HwL on web + 10 HwL on flange

HwD, HwL – Half wave Distortional, Local buckling

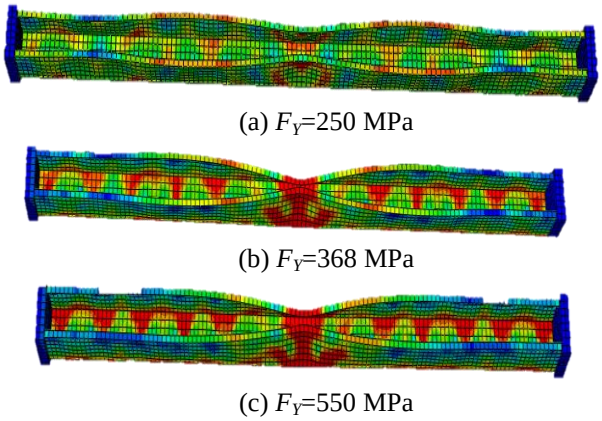

(a) F_Y=250 MPa

(b) F_Y=368 MPa

(c) F_Y=550 MPa

Fig. 4 Stress contours and failure Modes of LS-2-1200 section

to 0.1 times of the thickness of the section. On further load increment up to 20 kN, the local and distortional deformations did not seem to grow severe as expected. The section LS-2-1200 with yield stress 250 MPa showed strong L-D interaction with failure mode three half wave distortional buckling and several half wave local buckling on web and flanges as shown in Fig. 4(a). This section, failed at lower magnitude of distortional deformation, when flange-lip corner translational displacement is only 0.9 mm. The regions of web-flange corner and flange-lip corner at mid length section yielded first at 24.08 kN and subsequently the section failure is dominated by inner-inner distortional deformation at mid height. For section LS-2-1200 with yield stress 368 MPa, the first yield is at flange region near to flange-lip corner at load of 28.03 kN and subsequently the web-flange corner region at mid height and web started to yield at 28.98 kN, showing very strong L-D interaction mode buckling failure as shown in Fig 4b. The LS-2-1200 section with yield stress 550 MPa, behaviour is very similar to that of section with F_Y=368 MPa, until the occurrence of first yield at flange near flange-lip region at mid height, then the inner-inner distortional deformation grows severe, breaks down the three half wave distortional buckling to single half wave distortional buckling. The failure mode shown in Fig. 4c represents strong L-D interaction mode buckling. Hence, we can see that, though the L-D interaction has started at early stages of loading, the column may have considerable post buckling strength under L-D interaction buckling phenomenon. It can also be seen that as the yield to non-critical buckling ratio increases, the failure is very gradual

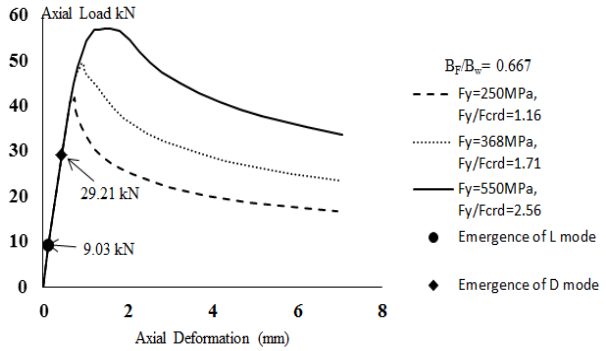

(a) Axial deformation versus axial load

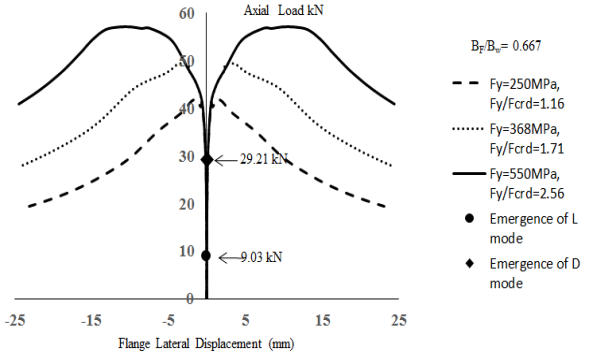

(b) Flange lateral deformation versus axial load

Fig. 5 Load versus deformation plot for section LS-3-800

with commendable resistance to loads even at large magnitude of deformations. The other column sections under Type 1 classification showed very similar behaviour like LS-2-1200 section and hence their post buckling behaviour is not presented here to avoid repetitions. The section LS-6-1600, initially developed four half wave distortional buckling followed by local and global (minor axis flexural buckling) respectively. Though the *G* mode critical stress is lesser than *D* mode as per GBTUL program, the first twenty eigenmodes obtained from FEA linear buckling analysis did not had *G* mode buckling. Hence, the initial geometrical imperfection assigned is combined *D* & *L* mode as shown in Table 3 rather than *G* mode.

4.1.2 Type 2 Sections

The sections with F_Y to F_{CRD} ratio greater than 1 and F_{CRD} to F_{CRL} ratio≥1.2 are classified as Type 2 sections as mentioned earlier. These sections are expected to incur secondary bifurcation L-D interaction mode buckling failure. A total of 47 sections out of 81 sections considered in this study belong to Type 2 category of sections. The post buckling behaviour of a column section LS-3-800 with F_Y=250, 368 & 550 MPa are presented. The column sections LS-3-800 have F_Y to F_{CRD} ratio of 1.16, 1.69 & 2.56 for yield stress 250, 368 & 550 MPa respectively and F_{CRD} to F_{CRL} ratio of 1.7. As mentioned earlier the column sections are analysed with minimal fixed load increments to identify the exact loads at emergence of *L* & *D* modes. As the initial geometrical imperfection for LS-3-800 column section is same for all three yield stresses the loads at emergence of *L* & *D* modes are very close. The loads versus

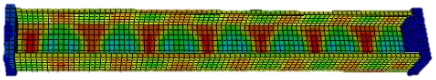

(a) Emergence of *L* deformation at 9.03 kN

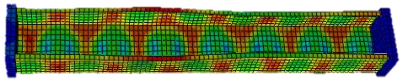

(b) Emergence of *D* deformation with prevalent *L* Deformation at 29.21 kN

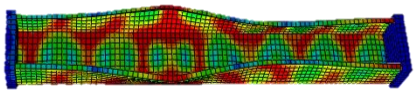

(c) Yield plateau & failure mode at 41.86 kN

Fig. 6 Stress contours and deformation modes of LS-3-800, F_Y=250 MPa column section

deformation plots for LS-3-800 with three different yield stresses are shown in Fig. 5(a) & (b). From Fig. 5(a) & (b) and Fig. 6(a) it can be seen that the seven half wave local buckling occurs first at load of 9.03 kN and subsequently only *L* mode is prevalent until the emergence of *D* mode at load of 29.21 kN. At 9.03 kN, the *L* mode deformation on web is higher than that of the flange. After the emergence of *D* mode at 29.21 kN, strong interactive behaviour between *L* & *D* modes is observed for section LS-3-800 with 250, 368 & 550 MPa. For the section with F_Y=250 MPa the failure is initiated by yielding of lip, web-flange junction region due to distortional deformations and yielding of web plate due to local deformations as shown in Fig. 6(c), which implies the failure is caused by both *L* & *D* modes interactively. For sections LS-3-800 with F_Y=368 & 550 MPa the *D* mode dominated the failure with formation of plastic hinges at flange-lip juncture. The behaviours of LS-3-800 sections are very similar to that of sections LS-2-1200 after the emergence of *L* & *D* mode. For LS-3-800 section with F_Y=250 MPa, the flange lateral displacement at ultimate load is very small (1.24 mm) and the failure is sudden. This might be certainly the effect of F_Y to F_{CRD} ratio. As the F_Y to F_{CRD} ratio increases the failure gets more gradual (Fig. 5, F_Y=550 MPa) with higher flange lateral deformations. From Fig. 5(a), it can be seen that no sudden reduction in stiffness or bifurcation point is visible at the emergence of *D* mode with prevalent *L* mode. Hence, based on the post buckling behaviour alone, the section LS-3-800 failing after secondary bifurcation L-D interaction mode buckling did not show significant differences on comparison with the section LS-2-1200 which fail after true L-D interaction mode buckling.

The initial geometrical imperfection is found to play significant role on the evolution of *L* & *D* modes. The post buckling behaviour of column sections LS-5-800 with different yield stresses are presented below as its buckling behaviour is found to be different from LS-3-800 section columns. The column sections LS-5-800 have F_Y to F_{CRD} ratio of 2.84, 4.18 & 6.26 for yield stress 250, 368 & 550 MPa respectively and F_{CRD} to F_{CRL} ratio of 1.97. Though the *L* & *D* critical stresses are significantly distinct, from Fig. 7(a) & (b) it can be noted that the emergence of both *L* & *D*

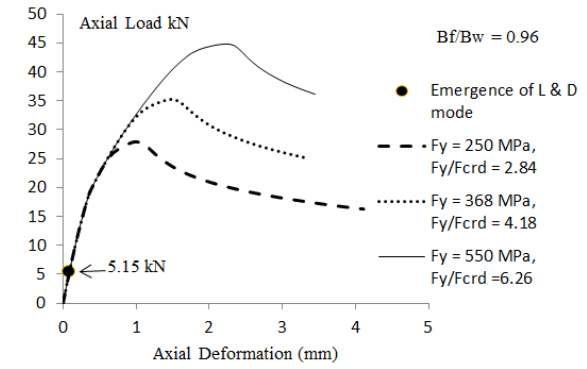

(a) Axial deformation versus axial load

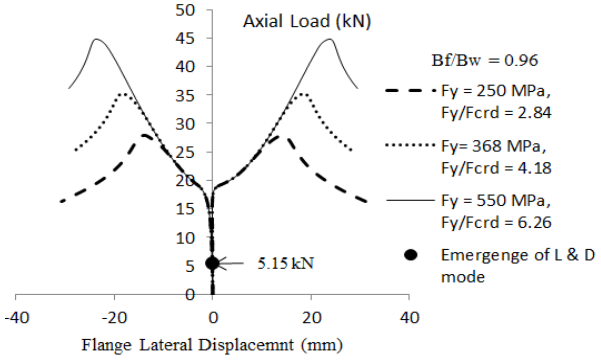

(b) Flange lateral deformation versus axial load

Fig. 7 Load versus deformation plot for section LS-5-800

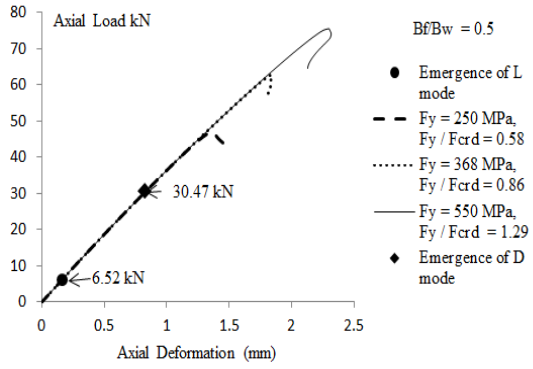

(a) Axial deformation versus axial load

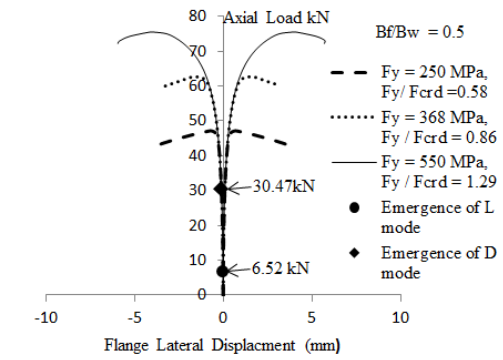

(b) Flange lateral deformation versus axial load

Fig. 8 Load versus deformation plot for section LS-4-1200

mode takes place at exactly same load (5.15 kN). The reason for the true L-D interaction might be due to the pre-defined initial geometrical imperfection. As the sections LS-5-800 have high F_Y to F_{CRD} ratios, the failure is observed to be gradual for the three different yield stresses considered (see, Fig. 7(a) & (b)). For LS-5-800 column section, at initial loads the flange translational displacements are asymmetric, that is up to 17.22 kN the left and right flanges lateral displacements are outer-inner respectively with unequal displacement magnitudes. On further load increments both the flanges showed outer-outer lateral displacements and at failure load both flanges deemed to have equal magnitude of lateral displacements. The LS-5-800 columns sections showed true L-D interaction mostly due to pre-defined initial geometrical imperfections. Also, from load-deformation equilibrium path, it can be understood that F_Y to F_{CRD} ratio strongly influences the post buckling behaviour of columns that fail after L-D interaction.

4.1.3 Type 3 Sections

The column sections with F_Y to F_{CRD} ratio≤1 and F_{CRD} to F_{CRL} ratio≥1.2 are classified as Type 3 sections in the present study. Amongst 81 column sections considered in this study, 19 column sections are Type 3 sections. The post buckling behaviour of column sections LS-4-1200 with F_Y= 250, 368 & 550 MPa are presented. The columns LS-4-1200 with yield stresses 250 & 368 MPa alone are Type 3 sections but for better understanding the behaviour of column with 550 MPa yield stress is also been reported. Fig. 8(a) & (b) shows the load versus deformation plots of LS-4-1200 column sections with different yield stresses. For this section the F_Y/F_{CRD} values are 0.58, 0.86 and 1.29 for 250, 368 & 550 MPa yield stresses respectively. In general, for column sections having F_Y/F_{CRD} ratio≤1 and F_{CRD}/F_{CRL} ratio≥1.5 the chances for occurrence of *D* mode buckling to interact with prevalent L mode is very less. The columns with this strength parametric ratios will predominantly fail by *L* mode buckling because the column cannot develop stresses equivalent to F_{CRD} which is beyond the yield stress of the material. For LS-4-1200 column section with F_Y=250 MPa, the F_Y/F_{CRD} ratio is just 0.58 which is very low and F_{CRD} to F_{CRL} ratio is 2.18 hence the participation of *D* mode with prevalent *L* mode looks very doubtful. But the post buckling analysis for LS-4-1200 columns section clearly shows the emergence of *D* mode with prevalent *L* mode. This column section having very less F_{CRL} value compared to its counterpart F_{CRD}, have pure *L* mode as most unfavourable imperfection (see Table 3) as expected yet shows strong L-D interaction mode buckling in load-deformation equilibrium path. As seen previously for column section LS-5-800, the early emergence of *D* mode probably due to pre-defined initial geometrical imperfection is eradicated in this case. The LS-4-1200 column sections do not have *D* mode deformation on their initial geometrical imperfection. From Fig. 8(a) & (b), it can be seen, the emergence of *L* mode buckling is at the load of 6.52 kN and emergence of *D* mode is at the load of 30.47 kN. The axial load versus axial deformation plot shown in Fig. 8(a) does not indicate any bifurcation on load-deformation equilibrium path on the emergence of *D* mode along with the prevalent *L* mode. The load-deformation

equilibrium path for LS-4-1200, LS-2-1200 with yield stress 250 MPa (Type 1 section) and LS-3-800 with yield stress 250 MPa (Type 2 section) are similar though their failure modes are different. The column sections of LS-2-1200 and LS-3-800 with F_Y=550 MPa showed gradual failure as their $F_Y/F_{CRD} \geq 2.5$, whereas the column sections LS-4-1200 for all three yield stresses showed sudden failure (see Fig. 8(a)) with less magnitude of *D* mode deformations (see Fig. 8(b)) due to low F_Y/F_{CRD} ratio. For LS-4-1200 column sections the lower magnitude of *D* mode deformation indicates the failure is predominant in *L* mode buckling.

5. Direct strength method design of columns

The specifications AISI S-100 and AS/NZ 4600 provides effective width method (EWM) and direct strength method (DSM) based design procedures for design of cold formed steel structural members. The DSM based design eradicates the limitations that the traditional EWM have like complex effective width calculations and unaccountability of web-flange juncture rotational stiffness for distortional buckling. The DSM based design was first proposed by Schafer and Pekoz (1998), it adopts Winter type strength curves to predict the nominal strength for columns and beams that fail after *L*, *D*, *G* (flexural, torsional and flexural-torsional) and L-G mode buckling. The DSM strength curves are developed based on the elastic buckling stresses obtained from finite strip analysis program and column strength data obtained from various experimental tests. The DSM design of cold formed steel members under compression and bending depends only on the elastic buckling stress and the yield stress values. The AISI S-100 specification provides limitations to use DSM design for members based on the cross sectional shape and dimensions. The column sections investigated in this paper have cross sectional shape and dimensions within the specified limits and belongs to pre-qualified columns category as per AISI S-100 for which DSM design can be conveniently adopted. All the column sections considered in this study have fixed ended boundary conditions and so the shift of effective centroid due to local buckling is neglected. As the equation prescribed by AISI to predict column nominal strength for local buckling includes L-G interaction mode buckling, the same equation is refined as given in Eq. (1a)-(1b) to calculate the column nominal strength for local buckling alone. The equation to predict column strength for distortional buckling as prescribed by AISI is given in Eqs. (2a)-(2b).

$$\begin{aligned} &for\ \lambda_L \leq 0.776 \\ &P_{NL} = P_Y \\ &for\ \lambda_L > 0.776 \end{aligned} \tag{1a}$$

$$P_{NL} = \left[1 - 0.15\left(\frac{P_{CRL}}{P_Y}\right)^{0.4}\right]\left(\frac{P_{CRL}}{P_Y}\right)^{0.4} P_Y \tag{1b}$$

where

$\lambda_L = \sqrt{\frac{P_Y}{P_{CRL}}}$ (non-dimensional local slenderness ratio)

P_{CRL} = critical elastic local column buckling load

P_Y = column squash load

P_{NL} = nominal strength of column for local buckling

$$\begin{aligned} &for\ \lambda_D \leq 0.561 \\ &P_{ND} = P_Y \\ &for\ \lambda_D > 0.561 \end{aligned} \tag{2a}$$

$$P_{ND} = \left[1 - 0.25\left(\frac{P_{CRD}}{P_Y}\right)^{0.6}\right]\left(\frac{P_{CRD}}{P_Y}\right)^{0.6} P_Y \tag{2b}$$

$\lambda_D = \sqrt{\frac{P_Y}{P_{CRD}}}$ (non-dimensional distortional slenderness ratio)

P_{CRD} = critical elastic distortional column buckling load

P_Y = column squash load

P_{ND} = nominal strength of column for distortional buckling

As the design specifications AISI S-100 and AS/NZ 4600 do not provide DSM column strength curve for columns failing under L-D interaction mode buckling phenomenon, the DSM based design procedures available from literature which includes interactive L-D mode buckling failure are used to calculate the nominal strength of the columns. Schafer (2002) suggested EWM and DSM based strength equations to include the various interactive modes buckling failure. Amongst them, the DSM based strength equation for columns failing after L-D interaction mode given in Eqs. (3a)-(3b) is adopted to calculate the nominal strength of the columns. Kwon *et al*. (2009) based on their experimental tests results modified the nominal strength equation for medium strength cold formed steel columns failing after L-D interaction mode buckling. The modified equation is given in Eqs. (4a)-(4b).

$$\begin{aligned} &for\ \lambda_{LD} \leq 0.776 \\ &P_{NLD} = P_{ND} \\ &for\ \lambda_{LD} > 0.776 \end{aligned} \tag{3a}$$

$$P_{NLD} = \left[1 - 0.15\left(\frac{P_{CRL}}{P_{ND}}\right)^{0.4}\right]\left(\frac{P_{CRL}}{P_{ND}}\right)^{0.4} P_{ND} \tag{3b}$$

where

$\lambda_{LD} = \sqrt{\frac{P_{ND}}{P_{CRL}}}$

P_{CRL} = critical elastic local column buckling load

P_{ND} = nominal strength of column for distortional buckling computed by Eqs. (2a)-(2b)

P_{NLD} = nominal strength of column for L-D interaction mode buckling

$$\begin{aligned} &for\ \lambda_{LD} \leq 0.667 \\ &P_{MNLD} = P_{ND} \\ &for\ \lambda_L > 0.667 \end{aligned} \tag{4a}$$

$$P_{MNLD} = \left[1 - 0.2\left(\frac{P_{CRL}}{P_{ND}}\right)^{0.4}\right]\left(\frac{P_{CRL}}{P_{ND}}\right)^{0.4} P_{ND} \tag{4b}$$

where

$\lambda_{LD} = \sqrt{\frac{P_{ND}}{P_{CRL}}}$ (non-dimensional L-D slenderness ratio)

P_{CRL} = critical elastic local column buckling load

P_{ND} = nominal strength of column for distortional buckling computed by Eqs.3 (a-b)

P_{MNLD} = modified nominal strength of column for L-D interaction mode buckling.

The DSM based column strength equation (NDL approach) to cater the L-D interaction mode buckling is proposed by Silvestre, Camotim and Dinis (2009) based on numerical investigation of simply supported columns. The DSM based NDL approach column strength equations are given in Eqs. (5a)-(5b). Silvestre, Camotim and Dinis (2012) based on their numerical investigation of fixed ended lipped channel columns modified the DSM based NDL approach. The modified NDL column strength equations are given in Eqs. (6a)-(6f). The DSM based column strength equations Eqs. (3)-(6), includes the column strength eroded by L-D interaction mode buckling, proposed based on the experimental and numerical investigations conducted mostly on lipped channel and web stiffened lipped channel column sections. Recently, Dinis, Young and Camotim (2014) and Martins *et al.* (2015, 2016) accessed the accuracy of strength predicted by NDL and modified NDL approaches based on experimental tests (rack and lipped channel column sections) and numerical investigations (lipped channel, web stiffened lipped channel, rack, Zed, hat column sections). As mentioned earlier, the DSM strength curves are explicit, as the column strengths are arrived purely on the basis of yield and critical buckling stresses of the column section. The literature studies concerning to L-D interaction buckling failure insists that the column sections investigated do not cover the entire possible ranges of the strength related parametric ratios and cross sectional shapes, hence the explicit nature of proposed DSM column strength curves needs to be assessed by conducting further studies (both experimental and numerical investigations) on a large amount of column sections that cover wide ranges of strength related parametric ratios and various cross sectional shapes. This study confines to only lipped channel column sections covering wide ranges of strength related parametric ratios.

$$\begin{gathered} for\ \lambda_{DL} \le 0.561 \\ P_{NDL} = P_{NL} \\ for\ \lambda_{DL} > 0.561 \end{gathered} \tag{5a}$$

$$P_{NDL} = \left[1 - 0.25\left(\frac{P_{CRD}}{P_{NL}}\right)^{0.6}\right]\left(\frac{P_{CRD}}{P_{NL}}\right)^{0.6} P_{NL} \tag{5b}$$

where

$\lambda_{DL} = \sqrt{\frac{P_{NL}}{P_{CRD}}}$ (non-dimensional D-L slenderness ratio)

P_{CRD} = critical elastic distortional column buckling load

P_{NL} = nominal strength of column for local buckling computed by Eqs. (1a)-(1b)

P_{NDL} = nominal strength of column for D-L interaction mode buckling

$$\begin{gathered} for\ \lambda_D \le 1.5 \\ P_{NDL} = P_{ND} \\ for\ \lambda_D > 1.5\ and\ \lambda_{DL} \le 0.561 \end{gathered} \tag{6a}$$

$$\begin{gathered} P_{MNDL} = P_{NL} \\ for\ \lambda_D > 1.5\ and\ \lambda_{DL} > 0.561 \end{gathered} \tag{6b}$$

$$P_{MNDL} = \left[1 - 0.25\left(\frac{P_{CRD}}{P^*_{NL}}\right)^{0.6}\right]\left(\frac{P_{CRD}}{P^*_{NL}}\right)^{0.6} P^*_{NL} \tag{6c}$$

Where

$$P^*_{NL} = P_Y \quad if\ \frac{L_{CRD}}{L_{CRL}} \le 4 \tag{6d}$$

$$\begin{gathered} P^*_{NL} = P_Y + (1 - 0.25\frac{L_{CRD}}{L_{CRL}})(P_Y - P_{NL}) \\ if\ 4 \le \frac{L_{CRD}}{L_{CRL}} \le 8 \end{gathered} \tag{6e}$$

and

$$P^*_{NL} = P_{NL} \quad if\ \frac{L_{CRD}}{L_{CRL}} \ge 8 \tag{6f}$$

$\lambda_D = \sqrt{\frac{P_Y}{P_{CRD}}}$ (non-dimensional distortional slenderness ratio)

$\lambda_{DL} = \sqrt{\frac{P_{NL}}{P_{CRD}}}$ (non-dimensional D-L slenderness ratio)

P_{NDL} = nominal strength of column for L-D interaction mode buckling

P_{ND} = nominal strength of column for distortional buckling computed by Eqs. (2a)-(2b)

P_{MNDL} = modified nominal strength of column for D-L interaction mode buckling

P_{CRD} = critical elastic distortional column buckling load

L_{CRL} = critical half wave local buckling length

L_{CRD} = critical half wave distortional buckling length

The column nominal strengths predicted by the DSM equations mentioned above in Eqs. (1)-(6), the yield stresses and squash loads for all columns are presented in Table 4.

6. Evaluation of DSM column strengths

6.1 Evaluation of DSM estimates based on ultimate strength from FEA

The accuracy of column strengths predicted by DSM equations P_{NL}, P_{ND}, P_{NLD}, P_{MNLD}, P_{NDL} and P_{MNDL} are evaluated based on the column ultimate strength data obtained from FEA analysis carried out in this study. The Table 5 reports the type of section, failure modes, FEA column failure loads ($P_{U,FEA}$) and the DSM predicted column strengths to $P_{U,FEA}$ ratios. (i) The current DSM P_{NL} strength curves predicts accurate strength estimates ($0.9 \le P_{NL}/P_{U,FEA} \le 1.05$) only for 16 column sections out of 81 columns considered in this study. The averages of the $P_{NL}/P_{U,FEA}$ ratio is 1.42 and standard deviation is 0.36 which shows the current DSM P_{NL} strength curve is unable to capture the column strength eroded by L-D interaction as reported by other researchers. (ii) The current DSM P_{ND} strength curves overestimate the column strengths for all the

Table 4 Nominal column strength predicted by DSM based strength equations

Section ID	F_Y MPa	P_Y kN	P_{CRL} kN	P_{CRD} kN	λ_L	λ_D	λ_{LD}	λ_{DL}	λ^*_{DL}	P_{NL} kN	P_{ND} kN	P_{MNLD} kN	P_{NLD} kN	P_{NDL} kN	P_{MNDL} kN
	250	64.25			1.40	1.19	1.13	0.98	1.01	43.46	41.50	30.89	32.61	33.11	34.29
LS-1-800	368	94.58	32.7	45.2	1.70	1.45	1.25	1.11	1.16	55.79	50.96	35.55	37.34	38.34	40.18
	550	141.3			2.08	1.77	1.38	1.26	1.34	72.20	62.33	40.75	42.61	44.23	46.98
	250	64.25			1.36	1.32	1.05	1.10	1.13	44.26	37.80	29.43	31.19	30.78	31.76
LS-1-1200	368	94.58	34.5	36.8	1.65	1.60	1.16	1.24	1.29	56.83	46.09	33.75	35.58	35.39	36.94
	550	141.35			2.02	1.96	1.27	1.41	1.49	73.58	56.08	38.59	40.49	40.59	42.93
	250	64.25			1.34	1.40	1.00	1.17	1.20	44.70	35.80	28.58	30.36	29.45	30.33
LS-1-1600	368	94.58	35.5	32.8	1.63	1.70	1.11	1.32	1.37	57.42	43.49	32.72	34.57	33.74	35.15
	550	141.35			1.99	2.07	1.22	1.50	1.59	74.35	52.78	37.37	39.29	38.59	40.72
	250	57.50			1.24	1.08	1.04	0.93	0.96	42.19	40.39	31.50	33.39	33.55	34.88
LS-2-800	368	84.64	37.1	49.1	1.51	1.31	1.16	1.05	1.10	54.27	49.99	36.50	38.47	39.06	41.26
	550	126.50			1.85	1.61	1.29	1.20	1.28	70.36	61.51	42.05	44.11	45.26	48.66
	250	57.50			1.21	1.22	0.97	1.05	1.08	42.92	36.42	29.75	31.67	30.87	31.95
LS-2-1200	368	84.64	39.0	38.7	1.47	1.48	1.07	1.19	1.25	55.23	44.65	34.29	36.30	35.62	37.43
	550	126.50			1.80	1.81	1.18	1.36	1.45	71.63	54.55	39.37	41.46	40.98	43.80
	250	57.50			1.21	1.27	0.94	1.10	1.13	43.07	35.18	29.12	31.05	29.96	30.97
LS-2-1600	368	84.64	39.4	35.9	1.46	1.53	1.04	1.24	1.30	55.43	43.01	33.52	35.53	34.49	36.20
	550	126.50			1.79	1.88	1.15	1.41	1.51	71.90	52.45	38.45	40.54	39.59	42.26
	250	79.50			1.40	1.08	1.18	0.89	1.00	53.68	56.06	40.53	42.68	44.14	51.42
LS-3-800	368	117.02	40.3	68.4	1.70	1.31	1.31	1.00	1.19	68.89	69.40	46.87	49.12	51.53	62.62
	550	174.90			2.08	1.60	1.46	1.14	1.42	89.16	85.42	53.90	56.25	59.84	75.97
	250	79.50			1.37	1.21	1.09	1.00	1.13	54.61	50.61	38.36	40.56	40.83	46.79
LS-3-1200	368	117.02	42.3	54.1	1.66	1.47	1.21	1.14	1.34	70.12	62.07	44.14	46.43	47.20	56.40
	550	174.90			2.03	1.80	1.34	1.29	1.60	90.78	75.86	50.58	52.96	54.38	67.88
	250	79.50			1.34	1.26	1.05	1.05	1.17	55.33	48.93	37.91	40.16	39.92	45.40
LS-3-1600	368	117.02	44.0	50.3	1.63	1.52	1.17	1.19	1.39	71.07	59.85	43.57	45.91	46.02	54.56
	550	174.90			1.99	1.86	1.29	1.35	1.67	92.03	73.00	49.89	52.33	52.90	65.52
	250	63.00			1.17	0.68	1.14	0.59	0.62	48.31	60.49	44.58	47.03	48.13	51.62
LS-4-800	368	92.74	46.3	138	1.41	0.82	1.32	0.67	0.71	62.21	80.29	54.08	56.67	59.88	65.84
	550	138.60			1.73	1.00	1.50	0.77	0.83	80.74	103.76	64.25	66.97	72.96	82.25
	250	63.00			1.13	0.77	1.07	0.68	0.70	49.35	56.91	43.59	46.13	47.33	50.02
LS-4-1200	368	92.74	49.3	107	1.37	0.93	1.22	0.77	0.81	63.59	73.60	52.02	54.69	57.29	62.02
	550	138.60			1.68	1.14	1.38	0.88	0.95	82.58	93.46	61.16	63.96	68.41	75.91
	250	63.00			1.12	0.80	1.05	0.71	0.73	49.57	55.59	43.06	45.61	46.68	49.18
LS-4-1600	368	92.74	49.9	99.3	1.36	0.97	1.20	0.80	0.85	63.88	71.41	51.17	53.85	56.13	60.55
	550	138.60			1.67	1.18	1.34	0.91	0.99	82.97	90.25	59.99	62.81	66.68	73.73
	250	103.75			2.37	1.69	1.61	1.15	1.40	48.15	48.02	28.32	29.44	32.14	39.88
LS-5-800	368	152.72	18.5	36.4	2.87	2.04	1.77	1.30	1.66	61.39	57.81	32.01	33.17	36.71	47.20
	550	228.25			3.51	2.50	1.94	1.47	1.98	78.98	69.65	36.17	37.38	41.88	55.99
	250	103.75			2.38	2.06	1.46	1.40	1.71	47.90	38.95	24.51	25.58	26.62	32.62
LS-5-1200	368	152.72	18.2	24.3	2.89	2.50	1.60	1.58	2.03	61.06	46.54	27.60	28.70	30.13	38.29
	550	228.25			3.54	3.06	1.75	1.79	2.42	78.55	55.75	31.10	32.24	34.11	45.09
	250	103.75			2.35	2.17	1.40	1.48	1.81	48.35	36.83	23.81	24.88	25.42	30.96
LS-5-1600	368	152.72	18.7	21.9	2.85	2.64	1.53	1.68	2.14	61.65	43.94	26.80	27.91	28.71	36.26
	550	228.25			3.49	3.23	1.68	1.90	2.55	79.32	52.56	30.18	31.33	32.45	42.64
	250	42.50			0.94	0.82	0.88	0.77	0.78	37.49	36.77	31.73	33.99	33.71	34.02
LS-6-800	368	62.56	47.5	62.9	1.15	1.00	0.99	0.88	0.89	48.50	47.00	37.74	40.12	40.13	40.87
	550	93.50			1.40	1.22	1.12	1.00	1.03	63.20	59.20	44.31	46.79	47.32	48.66
	250	42.50			0.93	0.88	0.85	0.83	0.84	37.81	35.06	30.89	33.17	32.46	32.73
LS-6-1200	368	62.56	48.8	54.6	1.13	1.07	0.95	0.95	0.96	48.93	44.36	36.52	38.92	38.32	38.97
	550	93.50			1.38	1.31	1.07	1.08	1.11	63.77	55.48	42.70	45.21	44.89	46.08

Table 4 Continued

Section ID	F_Y MPa	P_Y kN	P_{CRL} kN	P_{CRD} kN	λ_L	λ_D	λ_{LD}	λ_{DL}	λ^*_{DL}	P_{NL} kN	P_{ND} kN	P_{MNLD} kN	P_{NLD} kN	P_{NDL} kN	P_{MNDL} kN
	250	42.50			0.88	0.91	0.79	0.87	0.88	39.33	34.34	31.48	33.99	32.67	32.84
LS-6-1600	368	62.56	55.2	51.6	1.06	1.10	0.89	0.99	1.01	50.98	43.29	37.20	39.83	38.42	38.94
	550	93.50			1.30	1.35	0.99	1.14	1.16	66.53	54.00	43.49	46.23	44.86	45.87
	250	78.00			1.67	0.83	1.55	0.64	0.75	46.67	67.12	40.68	42.35	45.65	58.64
LS-7-800	368	114.82	28.0	113	2.02	1.00	1.75	0.73	0.89	59.74	85.69	47.82	49.58	55.55	74.09
	550	171.60			2.47	1.23	1.96	0.82	1.07	77.14	107.84	55.60	57.44	66.62	92.37
	250	78.00			1.65	0.92	1.48	0.71	0.84	46.97	62.34	38.96	40.63	44.00	55.07
LS-7-1200	368	114.82	28.6	91.9	2.00	1.12	1.66	0.81	0.99	60.14	78.45	45.40	47.15	52.57	68.45
	550	171.60			2.45	1.37	1.85	0.92	1.19	77.67	97.73	52.47	54.30	62.17	84.34
	250	78.00			1.61	0.96	1.42	0.75	0.88	47.73	60.39	38.71	40.43	43.57	53.70
LS-7-1600	368	114.82	29.9	84.5	1.96	1.16	1.59	0.85	1.04	61.13	75.63	44.99	46.79	51.71	66.36
	550	171.60			2.40	1.42	1.77	0.97	1.24	78.96	93.88	51.90	53.78	60.84	81.40
	250	68.40			1.42	0.74	1.37	0.60	0.67	45.77	63.10	41.51	43.42	45.46	54.90
LS-8-800	368	100.68	33.8	126	1.72	0.89	1.56	0.68	0.79	58.73	82.21	49.55	51.57	56.16	70.37
	550	150.48			2.11	1.09	1.76	0.78	0.95	75.99	104.91	58.22	60.34	68.09	88.57
	250	68.40			1.38	0.83	1.28	0.69	0.76	46.69	58.76	40.29	42.27	44.54	52.11
LS-8-1200	368	100.68	35.8	99.0	1.68	1.01	1.45	0.78	0.90	59.94	74.98	47.49	49.57	53.65	65.24
	550	150.48			2.05	1.23	1.62	0.88	1.07	77.59	94.32	55.34	57.52	63.84	80.73
	250	68.40			1.35	0.86	1.24	0.72	0.79	47.35	57.26	40.11	42.14	44.24	51.16
LS-8-1600	368	100.68	37.3	91.7	1.64	1.05	1.40	0.81	0.94	60.81	72.67	47.13	49.26	52.93	63.62
	550	150.48			2.01	1.28	1.56	0.93	1.12	78.73	91.06	54.80	57.03	62.66	78.36
	250	91.50			1.65	0.89	1.49	0.69	0.73	55.25	74.85	46.54	48.52	52.48	56.70
LS-9-800	368	134.69	33.8	114	2.00	1.08	1.67	0.78	0.84	70.74	94.58	54.36	56.44	63.00	69.18
	550	201.30			2.44	1.32	1.87	0.89	0.97	91.35	118.16	62.94	65.11	74.78	83.60
	250	91.50			1.63	1.00	1.42	0.78	0.82	55.54	68.67	44.14	46.11	49.68	53.25
LS-9-1200	368	134.69	34.3	91.6	1.98	1.21	1.58	0.88	0.94	71.11	85.65	51.15	53.21	58.70	63.95
	550	201.30			2.42	1.48	1.76	1.00	1.09	91.85	105.98	58.89	61.04	68.83	76.36
	250	91.50			1.60	1.11	1.33	0.87	0.91	56.38	63.01	42.23	44.24	46.95	49.95
LS-9-1600	368	134.69	35.7	74.5	1.94	1.34	1.47	0.98	1.05	72.22	77.82	48.67	50.77	54.84	59.29
	550	201.30			2.37	1.64	1.63	1.12	1.22	93.29	95.61	55.82	58.00	63.71	70.13

column sections. The averages of the $P_{ND}/P_{U,FEA}$ ratio is 1.39 and standard deviation is 0.14. A total of 43 column sections in this study have $\lambda_D \leq 1.5$, amongst them 12 columns have similar critical stresses. The P_{ND} strength curve clearly over estimates their strengths. The Eqs. 6(a) proposed by Silvestre *et al.* (2012) based on the numerical failure loads concerning to columns having similar critical stresses (true L-D interaction), do not comply with the results obtained in this study. (iii) The P_{NLD} strength curve predicts accurate strengths ($0.9 \leq P_{NLD}/P_{U,FEA} \leq 1.05$) for 27 column sections with an average $P_{NLD}/P_{U,FEA}$ ratio of 0.99 and standard deviation of 0.16. The average value of $P_{NLD}/P_{U,FEA}$ ratio shows that the DSM P_{NLD} strength curve can closely capture the strength erosion due to L-D interaction. However, the slightly higher standard deviation value implies that the P_{NLD} curve estimates are inaccurate (either very conservative or very unsafe) and scattered for many sections. (iv) The modified NLD approach predicts accurate strength estimates for 24 columns which is slightly lesser than the one predicted by NLD approach, with an average $P_{MNLD}/P_{U,FEA}$ ratio of 0.94 and standard deviation of 0.15. The modified NLD approach predicts over conservative estimates for more columns compared to that of columns with very unsafe strength estimates. (v) The P_{NDL} strength curve predicts accurate column strengths ($0.9 \leq P_{NLD}/P_{U,FEA} \leq 1.05$) for 43 sections with an average $P_{NDL}/P_{U,FEA}$ ratio of 1.03 and standard deviation of 0.13. Though the average of $P_{NDL}/P_{U,FEA}$ ratio is slightly above 1, the P_{NDL} strength curve predicts accurate strengths for more than 50 percent of the columns considered in this study. The strength estimates of NDL approach are superior as its standard deviation value is quite less than the other DSM estimates. (vi)The modified NDL strength curve is able to estimate accurate strength for only 14 columns which are lesser than the P_{NL} ones. The average $P_{MNDL}/P_{U,FEA}$ ratio is 1.17 and standard deviation of 0.12. It should be noted that for the calculation of modified NDL strength, the Eqs. 6(a) is disregarded as PND estimates are very unsafe for most of the columns with $\lambda_D \leq 1.5$. The Eqs. 6 (b)-6(c) are only used to calculate P_{MNDL}. The P_{MNDL} strength curve over estimates the column strength for most of the columns and hence the modified NDL approach unable to capture the adverse effect of L-D interaction mode buckling failure.

Table 5 Type of section, failure modes, FEA ultimate loads and comparison of DSM predicted strengths

Section ID	F_Y MPa	Type of Section	Failure Mode	$P_{U,FEA}$ kN	$P_{NL}/P_{U,FEA}$	$P_{ND}/P_{U,FEA}$	$P_{NLD}/P_{U,FEA}$	$P_{MNLD}/P_{U,FEA}$	$P_{NDL}/P_{U,FEA}$	$P_{MNDL}/P_{U,FEA}$
LS-1-800	250	2	L-D	29.21	1.49	1.42	1.06	1.12	1.13	1.17
	368	2	L-D	36.45	1.53	1.40	0.98	1.02	1.05	1.10
	550	2	L-D	45.63	1.58	1.37	0.89	0.93	0.97	1.03
LS-1-1200	250	1	L-D	24.93	1.78	1.52	1.18	1.25	1.23	1.27
	368	1	L-D	30.77	1.85	1.50	1.10	1.16	1.15	1.20
	550	1	L-D	39.79	1.85	1.41	0.97	1.02	1.02	1.08
LS-1-1600	250	1	L-D	22.06	2.03	1.62	1.30	1.38	1.33	1.37
	368	1	L-D	26.89	2.14	1.62	1.22	1.29	1.25	1.31
	550	1	L-D	42.77	1.74	1.23	0.87	0.92	0.90	0.95
LS-2-800	250	2	L-D	25.50	1.65	1.58	1.24	1.31	1.32	1.37
	368	2	L-D	31.41	1.73	1.59	1.16	1.22	1.24	1.31
	550	2	L-D	39.67	1.77	1.55	1.06	1.11	1.14	1.23
LS-2-1200	250	1	L-D	24.09	1.78	1.51	1.23	1.31	1.28	1.33
	368	1	L-D	28.48	1.94	1.57	1.20	1.27	1.25	1.31
	550	1	L-D	36.83	1.94	1.48	1.07	1.13	1.11	1.19
LS-2-1600	250	1	L-D	24.19	1.78	1.45	1.20	1.28	1.24	1.28
	368	1	L-D	27.23	2.04	1.58	1.23	1.30	1.27	1.33
	550	1	L-D	33.08	2.17	1.59	1.16	1.23	1.20	1.28
LS-3-800	250	2	L-D	41.35	1.30	1.36	0.98	1.03	1.07	1.24
	368	2	L-D	47.04	1.46	1.48	1.00	1.04	1.10	1.33
	550	2	L-D	57.06	1.56	1.50	0.94	0.99	1.05	1.33
LS-3-1200	250	2	L-D	35.69	1.53	1.42	1.07	1.14	1.14	1.31
	368	2	L-D	42.00	1.67	1.48	1.05	1.11	1.12	1.34
	550	2	L-D	56.65	1.60	1.34	0.89	0.93	0.96	1.20
LS-3-1600	250	2	L-D	36.92	1.50	1.33	1.03	1.09	1.08	1.23
	368	2	L-D	41.23	1.72	1.45	1.06	1.11	1.12	1.32
	550	2	L-D	53.16	1.73	1.37	0.94	0.98	1.00	1.23
LS-4-800	250	3	L-D	46.29	1.04	1.31	0.96	1.02	1.04	1.12
	368	3	L-D	58.28	1.07	1.38	0.93	0.97	1.03	1.13
	550	3	L-D	72.16	1.12	1.44	0.89	0.93	1.01	1.14
LS-4-1200	250	3	L-D	47.13	1.05	1.21	0.92	0.98	1.00	1.06
	368	3	L-D	62.23	1.02	1.18	0.84	0.88	0.92	1.00
	550	2	L-D	76.10	1.09	1.23	0.80	0.84	0.90	1.00
LS-4-1600	250	3	L-D	46.57	1.06	1.19	0.92	0.98	1.00	1.06
	368	3	L-D	63.21	1.01	1.13	0.81	0.85	0.89	0.96
	550	2	L-D	78.86	1.05	1.14	0.76	0.80	0.85	0.93
LS-5-800	250	2	L-D	27.55	1.75	1.74	1.03	1.07	1.17	1.45
	368	2	L-D	34.56	1.78	1.67	0.93	0.96	1.06	1.37
	550	2	L-D	44.58	1.77	1.56	0.81	0.84	0.94	1.26
LS-5-1200	250	2	L-D	23.93	2.00	1.63	1.02	1.07	1.11	1.36
	368	2	L-D	32.58	1.87	1.43	0.85	0.88	0.92	1.18
	550	2	L-D	45.88	1.71	1.22	0.68	0.70	0.74	0.98
LS-5-1600	250	2	L-D	26.98	1.79	1.37	0.88	0.92	0.94	1.15
	368	2	L-D	31.41	1.96	1.40	0.85	0.89	0.91	1.15
	550	2	L-D	43.97	1.80	1.20	0.69	0.71	0.74	0.97
LS-6-800	250	3	L-D	29.49	1.27	1.25	1.08	1.15	1.14	1.15
	368	3	L-D	38.25	1.27	1.23	0.99	1.05	1.05	1.07
	550	2	L-D	45.69	1.38	1.30	0.97	1.02	1.04	1.06

Table 5 Continued

Section ID	F_Y MPa	Type of Section	Failure Mode	$P_{U,FEA}$ kN	$P_{NL}/P_{U,FEA}$	$P_{ND}/P_{U,FEA}$	$P_{NLD}/P_{U,FEA}$	$P_{MNLD}/P_{U,FEA}$	$P_{NDL}/P_{U,FEA}$	$P_{MNDL}/P_{U,FEA}$
	250	3	L-D	28.72	1.32	1.22	1.08	1.16	1.13	1.14
LS-6-1200	368	2	L-D	36.97	1.32	1.20	0.99	1.05	1.04	1.05
	550	2	L-D	42.60	1.50	1.30	1.00	1.06	1.05	1.08
	250	1	L-D	28.55	1.38	1.20	1.10	1.19	1.14	1.15
LS-6-1600	368	1	L-D	35.52	1.44	1.22	1.05	1.12	1.08	1.10
	550	1	L-D-G	35.65	1.87	1.51	1.22	1.30	1.26	1.29
	250	3	L-D	50.26	0.93	1.34	0.81	0.84	0.91	1.17
LS-7-800	368	2	L-D	63.79	0.94	1.34	0.75	0.78	0.87	1.16
	550	2	L-D	78.94	0.98	1.37	0.70	0.73	0.84	1.17
	250	3	L-D	46.39	1.01	1.34	0.84	0.88	0.95	1.19
LS-7-1200	368	2	L-D	53.98	1.11	1.45	0.84	0.87	0.97	1.27
	550	2	L-D	72.68	1.07	1.34	0.72	0.75	0.86	1.16
	250	3	L-D	49.10	0.97	1.23	0.79	0.82	0.89	1.09
LS-7-1600	368	2	L-D	55.83	1.09	1.35	0.81	0.84	0.93	1.19
	550	2	L-D	67.40	1.17	1.39	0.77	0.80	0.90	1.21
	250	3	L-D	45.52	1.01	1.39	0.91	0.95	1.00	1.21
LS-8-800	368	3	L-D	57.27	1.03	1.44	0.87	0.90	0.98	1.23
	550	2	L-D	70.85	1.07	1.48	0.82	0.85	0.96	1.25
	250	3	L-D	44.80	1.04	1.31	0.90	0.94	0.99	1.16
LS-8-1200	368	2	L-D	54.26	1.10	1.38	0.88	0.91	0.99	1.20
	550	2	L-D	69.89	1.11	1.35	0.79	0.82	0.91	1.16
	250	3	L-D	47.30	1.00	1.21	0.85	0.89	0.94	1.08
LS-8-1600	368	2	L-D	59.94	1.01	1.21	0.79	0.82	0.88	1.06
	550	2	L-D	68.48	1.15	1.33	0.80	0.83	0.91	1.14
	250	3	L-D	55.10	1.00	1.36	0.84	0.88	0.95	1.03
LS-9-800	368	2	L-D	65.57	1.08	1.44	0.83	0.86	0.96	1.06
	550	2	L-D	80.65	1.13	1.47	0.78	0.81	0.93	1.04
	250	3	L-D	51.24	1.08	1.34	0.86	0.90	0.97	1.04
LS-9-1200	368	2	L-D	55.48	1.28	1.54	0.92	0.96	1.06	1.15
	550	2	L-D	65.49	1.40	1.62	0.90	0.93	1.05	1.17
	250	2	L-D	51.31	1.10	1.23	0.82	0.86	0.91	0.97
LS-9-1600	368	2	L-D	56.74	1.27	1.37	0.86	0.89	0.97	1.04
	550	2	L-D	61.96	1.51	1.54	0.90	0.94	1.03	1.13
				Mean	**1.42**	**1.39**	**0.99**	**0.94**	**1.03**	**1.17**
				S.D	**0.36**	**0.14**	**0.16**	**0.15**	**0.13**	**0.12**

6.2 Evaluation of DSM estimates based on experimental test data from literature

The experimental failure loads concerning to lipped channel columns sections failing after L-D interaction mode buckling phenomenon reported by Kwon *et al.* (2009), Loughlan *et al.* (2012), Young *et al.* (2013) are taken for the evaluation of DSM estimates. The experimental tests reported includes only of column sections with distinct critical buckling stresses. To the authors best knowledge there is no experimental test reports available on lipped channel columns with similar critical buckling stresses. The specimen Id, critical buckling stresses, yield stress, squash load, column ultimate load ($P_{U,EXP}$) and DSM predicted strengths to $P_{U,EXP}$ ratios are given in Table 6.

6.2.1 Kwon et al. (2009)

Kwon *et al.* (2009) conducted experimental tests on lipped channel, web stiffened or flange stiffened lipped channel column sections to study the effect of interactive behaviour on strength of columns. The column sections are made of high strength cold formed steel with yield stresses 627.7 MPa for 0.6 mm and 632.8 MPa for 0.8 mm thick sheets respectively. The experimental failure loads concerning to plain lipped channel column sections and the columns that failed after L-D interaction buckling are alone considered for this evaluation process. From Table 6 it can be seen that the all the sections of Kwon *et al.* (2009) have distinct *L* and *D* mode critical buckling stresses with non-dimensional distortional slenderness between 1.04 and 2.25. The current DSM P_{NL} and P_{ND} strength curves overestimate

Table 6 Specimen Id, critical stresses, yield stress, experimental failure loads and DSM estimates to failure loads ratio

	Specimen	F_{CRL} MPa	F_{CRD} MPa	F_Y MPa	P_Y kN	$P_{U,EXP}$ kN	λ_L	λ_D	P_{NL}/P_U	P_{ND}/P_U	P_{NLD}/P_U	P_{MNLD}/P_U	P_{NDL}/P_U
Young et al (2013)	T1.0-HSS-1	83	149	536	154.0	39.9	2.55	1.90	1.70	1.58	0.96	0.92	1.04
	T1.0-HSS-2	90	156	536	156.7	42.1	2.44	1.85	1.69	1.56	0.97	0.93	1.05
	T1.2-HSS-1	61	105	588	320.2	68.1	3.11	2.36	1.78	1.53	0.87	0.84	0.96
	T1.2-HSS-2	61	117	588	321.5	71	3.11	2.24	1.72	1.55	0.87	0.84	0.97
	T1.2-HSS-3	55	96	588	330.5	67.7	3.28	2.47	1.78	1.51	0.85	0.82	0.93
	T1.5-HSS-1	175	322	494	221.2	109	1.68	1.24	1.21	1.27	0.89	0.85	0.94
	T1.5-HSS-2	154	303	494	225.1	102.8	1.79	1.28	1.24	1.33	0.90	0.86	0.96
	T1.5-HSS-2R	157	311	494	227.8	103.6	1.77	1.26	1.26	1.35	0.92	0.88	0.98
	T1.5-HSS-3	45	82	494	457.5	92.9	3.31	2.45	1.78	1.54	0.85	0.83	0.94
	T1.5-HSS-4	44	95	494	453.5	94.7	3.35	2.29	1.72	1.61	0.86	0.84	0.98
	T1.9-MS-1	114	281	336	289.9	145.2	1.71	1.09	1.17	1.39	0.93	0.89	1.00
	T1.9-MS-2	113	307	336	286.9	146.1	1.72	1.04	1.15	1.42	0.93	0.89	1.01
	T1.9-MS-3	117	273	336	308.9	142.5	1.69	1.11	1.28	1.49	1.01	0.96	1.08
	T1.9-MS-5	255	471	336	246.5	170.8	1.15	0.84	1.12	1.23	1.00	0.95	1.03
	T1.9-MS-6	66	133	336	400.1	129.7	2.25	1.59	1.49	1.51	0.94	0.91	1.03
	T1.9-MS-7	66	147	336	397.9	131.6	2.26	1.51	1.45	1.56	0.95	0.91	1.05
	Average								**1.47**	**1.47**	**0.92**	**0.88**	**1.00**
	S.D								**0.26**	**0.12**	**0.05**	**0.05**	**0.05**
Loughlan et al (2012)	1	29	98	209	65.87	28.81	2.69	1.46	0.96	1.22	0.65	0.63	0.75
	2	29	100	209	65.87	31.52	2.69	1.45	0.88	1.12	0.60	0.58	0.69
	3	29	107	209	65.87	31.36	2.69	1.40	0.89	1.17	0.61	0.59	0.71
	4	29	123	209	65.87	31.77	2.69	1.31	0.88	1.23	0.63	0.61	0.74
	5	29	128	209	65.87	31.86	2.68	1.28	0.87	1.25	0.64	0.62	0.75
	6	39	112	209	57.46	29.80	2.30	1.37	0.91	1.10	0.64	0.61	0.72
	7	40	118	209	57.46	29.34	2.30	1.33	0.93	1.15	0.66	0.64	0.75
	8	40	120	209	57.46	30.00	2.29	1.32	0.91	1.13	0.65	0.63	0.73
	9	40	128	209	57.46	28.10	2.29	1.28	0.97	1.24	0.71	0.68	0.80
	10	40	150	209	57.46	29.50	2.29	1.18	0.93	1.27	0.70	0.68	0.81
	11	55	131	209	49.06	29.20	1.95	1.26	0.90	1.03	0.66	0.63	0.72
	12	55	132	209	49.06	26.76	1.95	1.26	0.98	1.13	0.72	0.69	0.79
	13	56	137	209	49.06	29.86	1.94	1.24	0.88	1.03	0.65	0.63	0.71
	14	56	144	209	49.06	30.11	1.93	1.21	0.88	1.04	0.66	0.63	0.72
	15	56	151	209	49.06	29.81	1.93	1.18	0.89	1.07	0.67	0.65	0.74
	16	84	166	209	50.30	29.10	1.58	1.12	1.07	1.18	0.84	0.80	0.88
	17	84	171	209	50.30	32.35	1.58	1.11	0.97	1.07	0.76	0.72	0.80
	18	84	176	209	50.30	29.80	1.58	1.09	1.05	1.18	0.83	0.79	0.88
	19	84	194	209	50.30	32.68	1.57	1.04	0.96	1.12	0.78	0.75	0.83
	20	85	223	209	50.30	29.80	1.57	0.97	1.06	1.30	0.89	0.85	0.95
	Average								**0.94**	**1.15**	**0.70**	**0.67**	**0.77**
	S.D								**0.06**	**0.08**	**0.08**	**0.08**	**0.07**
Kwon et al (2009)	A-6-1-400	172	553	627.7	52.73	20.66	1.91	1.07	1.38	1.82	1.07	1.11	1.23
	A-6-2-1000	109	153	627.7	62.52	14.01	2.40	2.02	2.05	1.71	1.06	1.11	1.16
	A-8-1-400	233	585	671.1	80.53	40.07	1.70	1.07	1.19	1.42	0.91	0.95	1.03
	A-8-2-400	304	615	671.1	75.16	33.49	1.48	1.04	1.46	1.62	1.12	1.18	1.24
	A-8-3-1000	100	256	671.1	96.64	30.10	2.60	1.62	1.39	1.55	0.85	0.88	0.99
	A-8-4-1000	99	133	671.1	91.27	22.63	2.60	2.25	1.74	1.38	0.85	0.88	0.92
	Average								**1.54**	**1.58**	**0.98**	**1.02**	**1.10**
	S.D								**0.31**	**0.17**	**0.12**	**0.13**	**0.13**

all the column strengths including the ones with $\lambda_D \leq 1.5$. This agrees well with the results obtained from the numerical investigation conducted in this study. Based on the averages of P_{NLD} and P_{MNLD} to $P_{U,EXP}$ ratios the P_{NLD} and P_{MNLD} strength curve predicts the column strengths pretty accurately with marginally unsafe and safe estimates respectively. The P_{NDL} strength curve predicts accurate strengths for 3 columns out of 6 columns considered but the average of $P_{NDL}/P_{U,EXP}$ ratio shows unsafe strength estimates. Hence, it can be noted that the performance of

DSM strength predictions made from this experimental tests matches closely with the one made from the numerical study.

6.2.2 Loughlan et al. (2012)

Loughlan *et al.* (2012) conducted experimental tests on 20 fixed ended lipped channel column sections consisting basically of four sections with different cross sectional dimensions and each of the sections having five different lengths. All the column sections tested have distinct L and D mode critical elastic stresses with F_{CRD}/F_{CRL} ratio greater than 1 and λ_D between 0.97 and 1.46. The comparison of strength predicted by DSM P_{NL} strength against experimental test failure loads shows that the P_{NL} estimates are too safe for 7 sections ($P_{NL}/P_{U,EXP}\leq 0.9$), accurate and safe for 10 sections ($0.9\leq P_{NL}/P_{U,EXP}\leq 1.0$) , accurate and slightly unsafe ($1<P_{NL}/P_{U,EXP}\leq 1.05$) for 1 section and inaccurate and unsafe for 2 sections. The overall average of $P_{NL}/P_{U,EXP}$ ratio of 0.94, shows that the strength erosion due to L-D interaction is insignificant or nil for the column sections investigated except for 2 sections. The performance of DSM P_{NL} estimates reported based on numerical tests conducted in this study and experimental tests by Kwon *et al.* (2009) do not agree with the performance evaluated based on the experimental tests by Loughlan *et al.* (2012). The P_{ND} strength curve over estimates the failure loads of all column sections as expected and agrees with the previously reported performance on DSM P_{ND} estimates. The DSM NLD, MNLD and NDL strength curves predicts over conservative strength estimates for all the column sections tested by Loughlan *et al.* (2012).

6.2.3 Young et al. (2013)

The experimental tests conducted by Young *et al.* (2013) includes 26 fixed ended lipped channel column sections intended to study the L-D interaction behaviour and to assess the quality of DSM predicted column strengths. Out of 26 column sections tested 16 columns failed after L-D interaction and only those sections are chosen for the evaluation of DSM estimates in the present study. All the column sections tested by Young *et al.* (2013) have F_{CRD}/F_{CRL} ratio greater than 1 and λ_D between 0.84 and 2.47. The DSM P_{NL} and P_{ND} strength curves over estimates the failure loads by large margin for all columns. The NLD and modified NLD curves underestimates the column strengths with an average of P_{NLD} and P_{MNLD} to $P_{U,EXP}$ ratio of 0.92 and 0.88 respectively. The DSM NDL approach with an average of P_{NDL} to $P_{U,EXP}$ ratio of 1.00 and standard deviation of 0.05, shows exceptional accuracy in the prediction of failure loads.

Hence, from the evaluations on the performance of DSM estimates made against the experimental test data from literature and the present numerical study it can be inferred that both evaluations are well accordant and shows that NDL approach performs better in predicting the accurate column strengths in comparison with other DSM estimates.

7. Effect of parameters on strength erosion

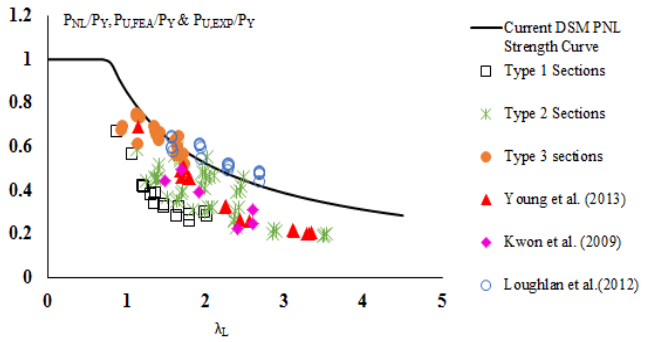

Fig. 9 Plot for P_{NL}/P_Y, $P_{U,FEA}/P_Y$, $P_{U,EXP}/P_Y$ versus λ_L

It is well proven and accepted that the current DSM P_{NL} and P_{ND} strength curves can accurately predict the column strengths for columns failing after pure L and pure D modes. This emphasises the fact, the effect of various parameters like F_{CRL}, F_{CRD}, yield stress, cross sectional shape and geometry on column strength is adequately addressed by the non-dimensional local and non-dimensional distortional slenderness ratio alone. Although, the NDL approach is identified to have better performance in terms of accurate strength prediction earlier, it is very important to note that the NDL approach predicts unsafe estimates for 27 columns considered in the present study. In other words the NDL estimates are unsafe for 32 percent of columns. This issue cannot be ignored and further studies are highly essential to arrive at the safe design rule. Hence one can say, for columns failing after the L-D interaction, the amount of strength erosion due to interactive buckling is associated to various parameters and the same cannot be adequately addressed by λ_{DL} alone. On this note, a brief analysis on parameters that can govern the degree of influence of L-D interaction mode buckling on column strength erosion is made. Here, to have a better understanding purpose the parameters are divided into two kinds namely (i) strength related parametric ratios and (ii) geometrical parameters.

7.1 Effect of strength related parametric ratios

The column sections classified earlier as Type 1, Type 2 and Type 3 sections based on their parametric ratios to study the post buckling mechanics are recalled here for the purpose of better understanding the role of parametric ratios on column strength erosion. The Fig. 9 shows the plot for P_{NL}/P_Y, $P_{U,FEA}/P_Y$ & $P_{U,EXP}/P_Y$ versus λ_L. From Fig. 9, it can be interpreted that the strengths of all column sections studied by Loughlan *et al.* (2012) are closely predicted by DSM P_{NL} strength curve. However, the strength of column sections studied by Kwon *et al.* (2009), Young *et al.* (2013) are over estimated by P_{NL} curve. The values of F_{CRL}, F_{CRD} and F_Y from Table 6 indicates, the column sections studied by above researchers belongs to Type 2 section ($F_Y/F_{CRD}>1$ and F_{CRD}/F_{CRL} ratio≥ 1.2) except for two column sections. For a total of 47 Type 2 sections considered in present study the P_{NL} curve predicts accurate strength ($0.9\leq P_{NL}/P_{U,FEA}\leq 1.05$) only for 4 column sections. Out of 19 Type 3 sections considered in present numerical study P_{NL} curve predicts

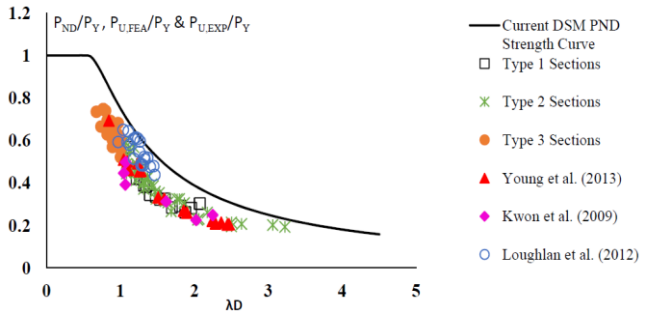

Fig. 10 Plot for P_{ND}/P_Y, $P_{U,FEA}/P_Y$, $P_{U,EXP}/P_Y$ versus λ_D

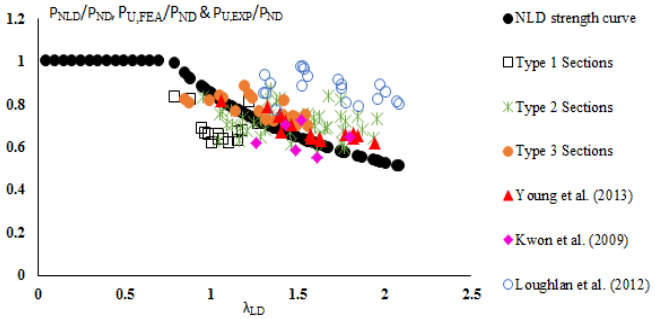

Fig. 11 Plot for P_{NLD}/P_{ND}, $P_{U,FEA}/P_{ND}$, $P_{U,EXP}/P_{ND}$ versus λ_{LD}

accurate strengths for 12 column sections, predicts 3 moderately unsafe strengths ($1.05<P_{NL}/P_{U,FEA}\leq 1.1$) and 3 highly unsafe strengths ($P_{NL}/P_{U,FEA}>1.1$). The strengths of all Type 1 column sections are over estimated by P_{NL} curve. The column strength erosion of Type 1 sections are very high and their $P_{U,FEA}/P_Y$ values are well aligned like Winter type curve. Hence it can be inferred that the P_{NL} curve predicts very unsafe estimates for Type 1 sections and hence cannot be adopted for design. For Type 2 (includes both experimental and numerical test columns) and Type 3 sections, the amount of strength erosion seems to vary which can be interpreted from the scatted $P_{U,FEA}/P_Y$ values and they do not match with Winter type curve alignment. Hence it can be inferred that for Type 2 and Type 3 sections the λ_L alone cannot adequately address the effect of various parameters. In addition, the consideration of strength related parametric ratios F_Y to F_{CRD} and F_{CRD} to F_{CRL} alone are not suffice to estimate the amount of strength erosion. Hence evaluation of other parameters concerning to column's cross sectional shape and dimensions are needed to be made for arriving at safe design rule concerning to L-D interaction failure. The Fig. 10 shows the plot for P_{ND}/P_Y, $P_{U,FEA}/P_Y$ & $P_{U,EXP}/P_Y$ versus λ_D. From Fig. 10, it is pretty clear that all the column strengths are over estimated by DSM P_{ND} strength curve. It is worth noting that, the columns $P_{U,FEA}/P_Y$ & $P_{U,EXP}/P_Y$ values are well aligned in accordance with Winter type curve. This shows the λ_D can address the effect of various parameters of column failing after L-D interaction though the P_{ND} curve cannot adequately predict the strength.

The Fig. 11 depicts the plot for P_{NLD}/P_{ND}, $P_{U,FEA}/P_{ND}$ and $P_{U,EXP}/P_{ND}$ versus λ_{LD}. From Fig. 11, the deficiency of λ_{LD} to handle the effect of various parameters is certainly proved. The $P_{U,FEA}/P_{ND}$ & $P_{U,EXP}/P_{ND}$ values are wide spread

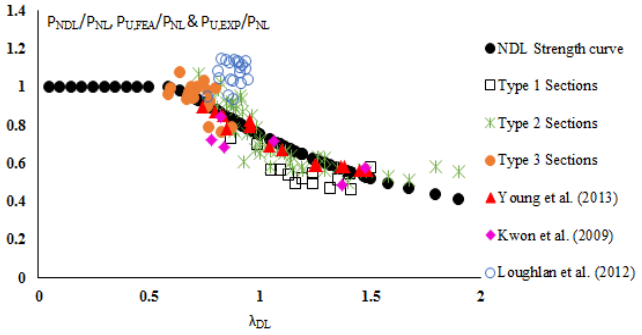

Fig. 12 Plot for P_{NDL}/P_{ND}, $P_{U,FEA}/P_{ND}$, $P_{U,EXP}/P_{ND}$ versus λ_{LD}

horizontally rather than forming Winter type alignment. The scattering of $P_{U,FEA}/P_{ND}$ & $P_{U,EXP}/P_{ND}$ values are due to inability of λ_L to include the effect of various parameters on column strength erosion. The NLD approach underestimates the column strengths for many of the Type 2 & Type 3 sections and overestimates the strengths for Type 1 sections. The Fig. 12 depicts the plot for P_{NDL}/P_{NL}, $P_{U,FEA}/P_{NL}$ and $P_{U,EXP}/P_{NL}$ versus λ_{DL}. From Fig. 12, it can be seen that the performance of NDL approach is better as the $P_{U,FEA}/P_{NL}$ & $P_{U,EXP}/P_{NL}$ values are less scattered and are aligned in accordance to Winter Type curve. The $P_{U,EXP}/P_{NL}$ values of Loughlan *et al.* (2012) sections forms cluster but this might be due to the fact that many of their sections have very close λ_{DL} values. The NDL approach overestimates the strength for most of the Type 1 sections. The $P_{U,EXP}/P_{NL}$ values of Young *et al.* (2013) column sections are well aligned along the NDL curve. The $P_{U,FEA}/P_{NL}$ & $P_{U,EXP}/P_{NL}$ values of Type 2 and Kwon *et al.*.(2009) column sections respectively are bit scattered. The NDL approach predicts safe and accurate strengths for Type 3 column sections except for 2 sections. Since the Type 3 sections covers only short range of λ_{DL} further study on Type 3 sections with wide ranges of λ_{DL} values are needed. Hence, the Figs. 9-12 confirms once again that DSM NDL approach is performing better in terms of accurate prediction of column strengths with comparatively less scattering of $P_{U,FEA}/P_{NL}$ & $P_{U,EXP}/P_{NL}$ ratios. The non-dimensional local slenderness ratio λ_L is unable to address the effect of various parameters on column strength erosion. The non-dimensional distortional slenderness ratio λ_D shows exceptional quality in addressing the effect of various parameters on column strength erosion.

7.2 Effect of section dimension

A brief study is made to see if the geometric parameters have significant effect on the column strength erosion due to L-D interaction mode buckling. The effect of the parametric ratio column flange plate width to web plate width (B_F/B_W) on column strength erosion alone is considered and the effect of other geometric parameters like various cross sectional shape, thickness, lip depth and column length are not addressed in this work. The Fig. 13 illustrates the plot for $P_{NDL}/P_{U,FEA}$ & $P_{NDL}/P_{U,EXP}$ versus B_F/B_W. From Fig. 13 it can be seen that the NDL approach predicts safe or very safe estimates for column sections with

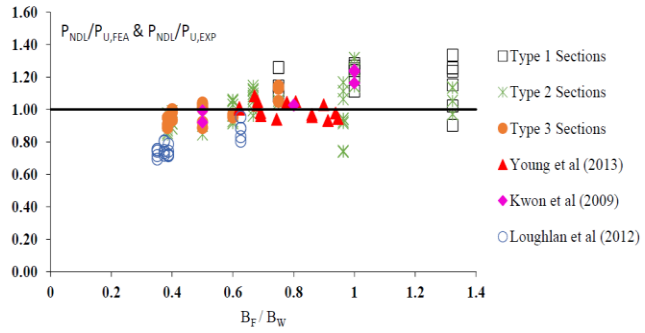

Fig. 13 Plot for $P_{U,FEA}/P_{NDL}$ & $P_{U,EXP}/P_{NDL}$ versus B_F/B_W

B_F/B_W ratio≤0.625. The column sections with B_F/B_W ratio≤ 0.625 includes, 16 Type 3, 20 Type 2 sections, 20 column sections tested by Loughlan *et al.* (2012), 2 column sections tested by Kwon *et al.* (2009) & 2 column sections tested by Young *et al.* (2013) column sections. Also, these sections covers a wide range of strength related parametric ratios like $0.45 \le F_Y/F_{CRD} \le 5.05$ and $1.34 \le F_{CRD}/F_{CRL} \le 4.4$. Hence, it can be inferred that for column sections with B_F/B_W ratio ≤0.625, the influence of strength related parametric ratios are less significant on column strength erosion and the NDL approach predicts conservative estimates. The reasons for over-conservative estimates by NDL for many of these columns sections are unknown and the other geometric parameters have to be included for detailed study. The Type 1 sections considered in this work does not have B_F/B_W ratio ≤0.625, hence studies are required to perform on the column sections with similar *L* & *D* critical elastic buckling stresses and B_F/B_W ratio ≤0.625 to assess the quality of NDL estimates.

The evaluation made on performances of NDL approach for column sections with B_F/B_W ratio ≥0.625 shows (i) the NDL approach predicts accurate strength estimates for most of the column sections tested by Young *et al.* (2013). Their column sections have F_Y/F_{CRD} ratio ranging between 0.71 and 5.58, F_{CRD}/F_{CRL} ratio between 1.72 and 2.33 and λ_{DL} between 0.74 and 1.49. (ii) For column sections tested by Kwon *et al.* (2009) the P_{NDL} curve predicts unsafe estimates. Their column sections have F_Y/F_{CRD} ratio ranging between 1.09 and 4.09, F_{CRD}/F_{CRL} ratio between 1.4 and 3.22 and λ_{DL} between 0.78 and 1.37. (iii) For column sections of Type 1, 2 and 3, considered in this study the NDL approach predicts unsafe estimates for most of the columns except for the columns with very high F_Y/F_{CRD} ratio (greater than 4). The NDL approach predicts highly unsafe estimates for Type 1 & 2 column sections with B_F/B_W ratio ≥1. From Fig. 13, the overlap of $P_{NDL}/P_{U,FEA}$ & $P_{NDL}/P_{U,EXP}$ values belonging to Type 1, 2 and Kwon *et al.* (2009) column sections with B_F/B_W ratio ≥1 can be seen. Hence, the evaluation of NDL approach based on parametric ratio B_F/B_W shows that, for column sections with B_F/B_W ratio ≤0.625, the influence of L-D interaction on strength erosion is low and the NDL approach under-estimates the column strengths. For column sections with B_F/B_W ratio ≥0.625, the column strength erosion due to L-D interaction is high and the NDL approach predicts unsafe estimates. This finding provides zest to carry out further studies to improve the NDL approach by considering the effect of B_F/B_W ratio.

8. Conclusions

The numerical investigation on fixed ended lipped channel column sections failing after L-D interaction mode buckling failure is reported. The identification of column section geometries using GBTUL programme is presented. The numerical investigation is carried out in FEA software ABAQUS. The FEA modelling procedures of identified column sections is explained and the same is validated against a section reported in the literature. The FEA includes linear and non-linear buckling analysis. The non-linearity of material is defined using ideal elastic-plastic stress-strain model. The geometrical non-linearity is defined by incorporating perturbed mesh associated to most unfavourable eigenmode obtained through linear analysis with imperfection magnitude of 1T. Then the identified column sections are classified into three types namely Type 1, Type 2 and Type 3 based on their strength related parametric ratios F_{CRD}/F_{CRL} & F_Y/F_{CRD} to study the post buckling mechanics involved. The emergence of *L* & *D* modes on the load-deflection equilibrium paths are illustrated along with deformation and stress contour plots for all the three types. The current DSM based strength curve available in AISI S-100 and the DSM based strength curves to cater the strength erosion due to L-D interaction mode buckling failure available in literatures are presented. Evaluation on performance of DSM based strength curves based on the column failure load data obtained from numerical investigation conducted in this study and from experimental tests reported in literature is carried out. Then, the effects of strength and geometry (only flange width and web width) related parameters on column strength erosion due to L-D interaction are studied.

From the works carried out the important findings are discussed below.

(i) The identification of column sections prone to secondary bifurcation kind L-D interaction is very difficult. In this study, the column sections are identified based on repetitive buckling analyses using code GBTUL.

(ii) The post buckling behaviour of columns undergoing true L-D interaction and secondary bifurcation kind L-D interaction are more or less similar. The columns with secondary bifurcation L-D interaction do not show bifurcation of axial load-axial deformation equilibrium paths at the emergence of *D* mode with prevalent *L* mode.

(iii) The columns with low F_Y to F_{CRD} values display high instability even at very small flange lateral (distortional) deformations and failure takes place suddenly.

(iv) The columns with high F_Y to F_{CRD} values display stable behaviour even with large flange lateral (distortional) deformations and failure is gradual with ample warning.

(v) The evaluation made on performance of DSM

strength curves implies the current DSM P_{NL} and P_{ND} strength curves certainly not able to cater the column strength erosion due to L-D interaction buckling. Amongst the various DSM strength curves proposed by several researchers, only the NDL approach proposed by Silvestre *et al.* (2012) provides column strength estimates satisfactorily.

(vi) The study made on effect of strength related parameters on column strength erosion implies the λ_L is not capable to adequately include the effects of various parameters on column strength erosion. Whereas, the λ_D can efficiently address the effects of various parameters but the P_{ND} strength curve provides unsafe estimates.

(vii) The NDL approach has to be refined further to overcome the danger of unsafe column strength predictions. One of the methods to improve the NDL approach is to include the B_F/B_W ratio because it is seen that the ratio plays significant role in column strength degradation due to L-D interaction buckling.

(viii) As the λ_D is seen to perform exceptionally well in terms of addressing the effects of various parameters in column strength degradation due to L-D interaction, the authors suggests to change only the P_{ND} strength equation without including the λ_L parameter for accurate prediction of column strength failing after L-D interaction mode buckling.

Acknowledgements

The first and second authors gratefully acknowledge VIT University, Vellore for the support through Seed Grant for Research.

References

ABAQUS (Computer software), ABAQUS Standard User's Manual, Version 6.12, Providence, RI, Dassault Systèmes Simulia.

AISI S100 (2007), North American Specification for the Design of Cold-formed Steel Structural Members, American Iron and Steel Institute (AISI), Washington, DC.

Ajeesh, S.S. and Jayachandran, A. (2017), "A constrained spline finite strip method for mode decomposition of cold-formed steel sections using GBT principles", *Thin Wall. Struct.*, **113**, 83-93.

Anbarasu, M. (2016), "Local-distortional buckling interaction on cold-formed steel lipped channel beams", *Thin Wall. Struct.*, **98**, 351-359.

AS/AZ 4600 (2005), Australian/New Zealand Standard for Cold-formed Steel Structures, Second Edition, Sydney-Wellington.

Bebiano, R., Silvestre, N. and Camotim, D. (2008), "GBTUL-A code for the buckling analysis of cold-formed steel members", *Nineteenth International Specialty Conference on Cold-Formed Steel Structures*, St. Louis, Missouri, U.S.A, October.

Davies, J.M. and Leach, P. (1992), "Some applications of generalized beam theory", *Eleventh International Specialty Conference on Cold-Formed Steel Structures*, St. Louis, Missouri, U.S.A, October.

Dinis, P.B., Young, B. and Camotim, D. (2014), "Local-distortional interaction in cold-formed steel rack-section columns", *Thin Wall. Struct.*, **81**, 185-194.

Gioncu, V. (1994), "General theory of coupled instabilities", *Thin Wall. Struct.*, **19**, 81-127.

Hancock, G.J. (2003), "Cold formed steel structures", *J. Constr. Steel Res.*, **59**, 473-487.

He, Z., Zhou, X., Liu, Z. and Chen, M. (2014), "Post-buckling behaviour and DSM design of web-stiffened lipped channel columns with distortional and local mode interaction", *Thin Wall. Struct.*, **84**, 189-203.

Kumar, M.A. and Kalyanaraman, V. (2014), "Distortional buckling of CFS stiffened lipped channel compression members", *J. Struct. Eng.*, **140**(12), 04014099.

Kwon, Y.B. and Hancock, G.J. (1992), "Tests of cold-formed channels with local and distortional buckling", *J. Struct. Eng.*, **117**(7), 1786-1803.

Kwon, Y.B., Kim, B.S. and Hancock, G.J. (2009), "Compression tests of high strength cold-formed steel channels with buckling interaction", *J. Constr. Steel Res.*, **65**, 278-289.

Kwon, Y.B., Kim, N.G. and Kim, B.S. (2005), "A study on direct strength method for compression members undergoing mixed mode buckling", *International Proceedings Of Steel Structures ISSS'05*, Seoul, Korea.

Loughlan, J., Yidris, N. and Jones, K. (2012), "The failure of thin-walled lipped channel compression members due to coupled local-distortional interactions and material yielding", *Thin Wall. Struct.*, **61**, 14-21.

Martins, A.D., Camotim, D., Dinis, P.B. and Young, B. (2015), "Local-distortional interaction in cold-formed steel columns: mechanics, testing, numerical simulation and design", *Struct.*, **4**, 38-57.

Martins, A.D., Dinis, P.B. and Camotim, D. (2016), "On the influence of local-distortional interaction in the behaviour and design of cold-formed steel web-stiffened lipped channel columns", *Thin Wall. Struct.*, **101**, 181-204.

Martins, A.D., Dinis, P.B., Camotim, D. and Providência, P. (2015), "On the relevance of local-distortional interaction effects in the behaviour and design of cold-formed steel columns", *Comput. Struct.*, **160**, 57-89.

Mulligan, G P. and Pekoz, T. (1987), "Local buckling interaction in cold-formed columns", *J. Struct. Eng.*, **113**(3), 604-620.

Narayanan, S. and Mahendran, M. (2003), "Ultimate capacity of innovative cold-formed steel columns", *J. Constr. Steel Res.*, **59**(4), 489-508.

Sadovský, Z., Kriváček, J., Ivančo, V. and Ďuricová, A. (2012), "Computational modelling of geometric imperfections and buckling strength of cold-formed steel", *J. Constr. Steel Res.*, **78**, 1-7.

Schafer, B.W. (2002), "Local, distortional and Euler buckling of thin-walled column", *J. Struct. Eng.*, **128**(3), 289-299.

Schafer, B.W. (2006), "Review: The direct strength method of cold-formed steel member design", *Stability And Ductility of Steel Structures*, Lisbon, Portugal, September.

Schafer, B.W. and Peköz, T. (1998), "Computational modelling of cold-formed steel: characterizing geometric imperfections and residual stresses", *J. Constr. Steel Res.*, **47**, 193-210.

Schafer, B.W., Li, Z. and Moen, C.D. (2010), "Computational Modelling of cold-formed steel", *Thin Wall. Struct.*, **48**, 752-762.

Silvestre, N., Camotim, D. and Dinis, P.B. (2009), "Direct strength prediction of lipped channel columns experiencing local-plate/distortional interaction", *Adv. Steel Constr.*, **5**(1), 49-71.

Silvestre, N., Camotim, D. and Dinis, P.B. (2012), "Post-buckling behaviour and direct strength design of lipped channel columns experiencing local/distortional interaction", *J. Constr. Steel Res.*, **73**, 12-30.

Yang, D. and Hancock, G.J. (2004), "Compression tests of high strength steel channel columns with interaction between local and distortional buckling", *J. Struct. Eng.*, **130**(12), 1954-1963.

Young, B. and Yan, J. (2002), "Channel columns undergoing local,

distortional and overall buckling", *J. Struct. Eng.*, **128**(6), 728-736.

Young, B., Silvestre, N. and Camotim, D. (2013), "Cold-formed steel lipped channel columns influenced by local-distortional interaction: strength and DSM design", *J. Struct. Eng*., **139**(6), 1059-1074.

Zeinoddini, V.M. and Schafer, B.W. (2012), "Simulation of geometric imperfections in cold-formed steel members using spectral representation approach", *Thin Wall. Struct.*, **60**, 105-117.

CC